Daniela Rainer, BSc

Kinetic resolution of DL-mandelic acid with a mutant variant of lactate oxidase from *Aerococcus viridians.*

Masterthese

zur Erlangung des akademischen Grades eines

Master of Science

der Studienrichtung Biotechnologie

erreicht an der

Technischen Universität Graz

Betreut duch:

Univ.-Prof. Dipl.-Ing. Dr. Bernd Nidetzky und

Institut für Biotechnologie und Bioprozesstechnik

2012

STATUTORY DECLARATION

I declare that I have authored this thesis independently, that I have not used other than the declared sources / resources, and that I have explicitly marked all material which has been quoted either literally or by content from the used sources.

…………………………   …………………………………………………..

            date   (signature)

I. Danksagung

An dieser Stelle möchte ich mich bei all jenen Menschen bedanken, die in persönlicher und fachlicher Hinsicht zu dem Gelingen dieser Masterarbeit beigetragen haben.

Mein ganz besonderer Dank gilt meinem Betreuer Dipl.-Ing. Dr. techn. Bernd NIDETZKY, ohne dessen Unterstützung und Leitung diese Arbeit nicht zustande gekommen wäre.

Ein ganz großes Dankeschön möchte ich auch an Professor Dr. David K. Wilson richten, der mir während der Zeit in den Vereinigten Staaten als Betreuer und Ratgeber zur Seite stand.

Einen besonderen Dank möchte ich an die Mitarbeiter des Institutes für Biotechnologie und Bioprozesstechnik aussprechen: die Unterstützung, Diskussionen und so manch aufbauendes Wort haben es ermöglicht diese Arbeit zu beenden.

Weiters möchte ich mich am Research Center of Pharmaceutical Engineering und Roche Diagnostics für die Finanzierung und die Aufgabenstellung bedanken.

Außerdem möchte ich ein Dankeschön an die LOX-Gruppe, Thomas Stoisser, Stephanie Gärtner, Birgit Unterweger und Daniela Neuhold richten. Die Zusammenarbeit mit euch war mir eine Freude.

Ein ganz spezielles Dankeschön an meine Eltern, Siegfried und Brigitte, meine Geschwister, Angelika und Cornelia und deren Lebenspartner, Thomas und Andreas sowie meinem Partner, Martin für die Unterstützung und den Zusammenhalt, den ich in dieser Familie erfahren darf.

Meinem bestem Freund, Florian, danke ich dafür, dass er da ist wenn ich ihn brauche.

II.   Kurzfassung

L-Laktat Oxidase (LOX) aus *Aerococcus viridians* ist ein Mitglied der Familie der Flavoenzyme, welche die Oxidation von L-α-Hydroxysäuren katalysieren. Diese Gruppe von Enzymen beinhalten Flavinmononucleotid (FMN) als deren prosthetische Gruppe. Dabei wird, einem Ping-Pong Mechanismus folgend, die Hydroxysäure in die korrespondierende Ketosäure unter Bildung von Wasserstoffperoxid umgewandelt.

Die Strategie eine Mutante zu kreieren, die keinerlei Einbußen in der Aktivität in Bezug auf L-Laktat, welches das natürliche Substrat der L-Laktat Oxidase ist, jedoch eine erhöhte Substratspezifität besitzt wurde durch eine Punkt-Mutation an Position 95 durchgeführt. Hierbei wurde Alanin gegen Glyzin ausgetauscht (A96G).

Durch kinetische Untersuchungen wurde herausgefunden, dass die Aktivität in Bezug auf langkettige α-Hydroxysäuren und α-Hydroxy-n-buttersäure als auch bei aromatischen α-Hydroxysäuren und L-Mandelsäure gesteigert wurde.

Weitere kinetische Experimente zeigten, dass die Mutante A95G von D-Mandelsäure nicht inhibiert wird. Im Wildtyp der LOX ist dies jedoch der Fall. Daher ist es möglich, L-Mandelat aus dem razemischen Gemisch heraus selektiv umzusetzen. Durch die strikte Stereospezifität der LOX wird in der Reaktion nur L-Mandelsäure als Substrat akzeptiert. Die Mutante A95G zeigt dieselbe Stereospezifität. Aufgrund dieser Resultate wurde versucht das razemische Gemisch der DL-Mandelsäure mit Hilfe dieser Mutante zu trennen.

In einer „one-pot chemo-enzymatic de-Racemization" wird die L-konfigurierte Mandelsäure durch die LOX A95G zu8 Phenylglyoxalsäure (PGA) und Wasserstoffperoxid (H_2O_2) oxidiert. Durch Zugabe von Natriumborhydrid ($NaBH_4$) wird PGA zu D-und L-Mandelsäure zu gleichen Teilen reduziert.

III.   Abstract

L-lactate oxidase (LOX) from *Aerococcus viridians* is a member of the group of flavoproteins, which catalyses the oxidation of L-α-hydroxyacids. This group of enzymes contains flavin-mononucleotide (FMN) as their prosthetic group. They are processing the substrate into the corresponding keto-acid and hydrogen peroxide following the Ping-Pong mechanism.

The strategy to create a mutant which has no decrease in activity for L-lactate, which is the natural substrate of LOX, but increased substrate specificity, was done via a point-mutation at the position Alanine95 to Glycine (A95G). During kinetic characterization it was found that the activity for long-chain α-hydroxyacids and α-hydroxy-n-butyric acid as well as aromatic α-hydroxyacids and L-mandelic acid was increased.

Further investigations in kinetics showed that the mutant A95G is not inhibited by D-mandelic acid, which is the case in the wild type (WT) LOX and therefore has the ability to selectively process L-mandelic acid in a racemic mixture. Because of the strict stereospecificity of the LOX, a reaction with D-mandelate is not occuring. Because of these results, the trial to separate the racemic mixture of DL-mandelic acid makes sense.

In a one-pot-chemo-enzymatic de-racemization experiment the L-form of mandelic acid is oxidized to phenylglyoxylic acid (PGA), the corresponding keto-acid of mandelic acid, and hydrogen peroxide (H_2O_2). The PGA is in presence of $NaBH_4$ reduced to D-and L-mandleic acid, respectively.

IV. Table of Content

1. Introduction

L-lactate oxidase (LOX) from *Aerococcus viridans* catalyzes the oxidation of L-lactate oxidase to pyruvate and hydrogen peroxide by using molecular oxygen. It is a member of α-hydroxyacid-oxidase flavoenzymes which is a well-studied enzyme family in mechanism and structure.

Lactate is a very important metabolite in various organisms. Several chemical, enzymatic, and microbial methods have been developed for the production of the enantiomer, where D-lactate is much more difficult to produce than the L-enantiomer [Oikawa et al., 2000].

It is mainly used in biosensors for the determination of L-lactate levels in medical and food analytics. The use of biosensors shows suitable for biotechnology approaches due to their good selectivity, fast response, miniature size, and reproducible results [Huang et al., 2008].

One cross-reaction of L-lactate oxidase with an alternative substrate, which is of particular interest in medical science, is the oxidation of glycolic acid. Glycolic acid is generated during the primary metabolism of ethylene glycol in the liver by ADH. The ingestion of ethylene glycol leads to ethylene glycol poisoning, which is a medical emergency. A reaction of glycolic acid with LOX in blood gas analyzers may induce false elevation of blood lactate and therefore a false diagnosis and medical treatment.

The aim of this work was to use a mutated variant of LOX, which has a broader substrate specificity, for deracemization of DL-mandelic acid. Further on, solving of the structure and clarification of the better substrate specificity was done.

1.1. L-lactate oxidase from *Aerococcus viridans* – mechanistic and structural work

The L-lactate oxidase (LOX; PDB code 2DU2) from *Aerococcus viridians* (*Av*) belongs to the family of flavoproteins, which are FMN-dependent and catalyze the oxidation of L-α-hydroxyacids. The enzymatic reaction proceeds via a ping-pong mechanisms, where in the reductive half reaction, the α-hydroxyacid substrate is oxidized to form a keto acid, and the flavin is reduced to the hydroquinone. In the oxidative half reaction, the reduced flavin is re-oxidized by an electron acceptor.

The LOX enzyme utilizes L-lactate and oxygen as substrates, similar to the lactate monooxygenase, but instead of acceleration of the decarboxylation of the products, pyruvate and hydrogenperoxide (H_2O_2) to acetic acid, carbon dioxide and water, it forms pyruvate and H_2O_2 as the final products (Figure 1). [Yorita, K. et al., 1997].
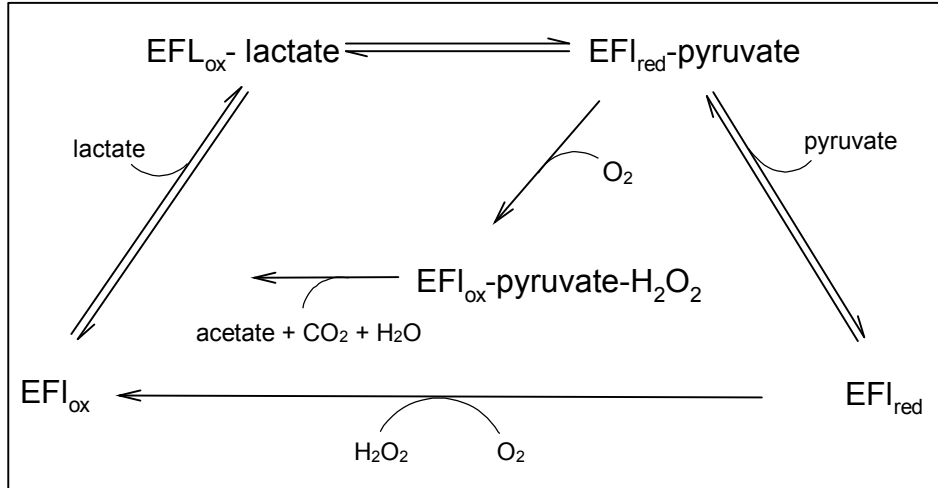
Figure 1: Reaction mechanism of LOX (outer pathway) and lactate monooxygenase (inner pathway).

A considerable amount of mechanistic work has been carried out extensively over the last three decades by various scientists [Cornforth, 1959; Ghisly et al., 1980; Rao et al., 1998; Dewanti et al., 2003; Cunane et al., 2005; Mattevi et al., 1996; Sobrado et al., 2003; Yorita et al., 1997] who described this mechanism as a carbanion mechanism, in which the substrate α-proton is abstracted by an active site base and the electrons from the resulting substrate carbanion are transferred to the flavin, which serves as the prosthetic group for these enzymes. Further investigations by Walsh et al. [Walsh et al., 1971; Walsh et al., 1973] demonstrated that the enzymes D-amino acid oxidase (DAO) and LOX catalyze the elimination of halide from β-halogeno substrate analogs. However, LOX showed an irreversible inactivation by the suicide substrate α-hydroxybutynoic acid [Ghisla et al., 1976; Schonbrunn et al., 1976]

It was also found that small anionic molecules act as competitive inhibitors of LOX, which can be divided in two classes [Ghisla et al., 1977], monoanionic acids and dianionic acids. Negative charges are located at one site (phosphate, sulfate, carbonate) in the class of monoanionic acids. Within the class of dianionic acids (oxalate, malonate and its derivatives) the negative charges are separated and showed a much tighter binding. Studies on function of pH showed that there is a specific dependence of K_d on the distance separating the negative charges of the LOX inhibitors which suggested that they are transition state analogs.

A comparison of the structures with that of the postulated transient substrate α-carbanion revealed that they have a similar location of the charges. The negative charge of the carboxylate function of the substrate will be neutralized by a protein counterion, which resulted in a formal protonation of the group and with this knowledge the contribution of lowering the energy the transition α-carbanion could be assumed. During the electron transfer step the negative charge would be transferred from the substrate carbanion to the reduced flavocoenzyme. In the state of the reduced enzyme-product complex, which is dissociating very slowly, two negative charges would be present at the active center. Therefore the reduced flavin can be suggested to function as a "charge

sink" and further to stabilize the enzyme in the transition state in presence of an appropriate distributed counterion in the active site [Ghisla et al., 1977].

These conclusion has been confirmed by the crystal structure of glycolate oxidase (GLO; PDB code 1GOX), where a lysine residue is orientated to the flavin N(1)-C(2)O locus. The FMN is located at the C-terminal end of the β-strands. Here, amino acid residues form the binding pocket for the co-factor and are well-conserved at the top of the barrel.
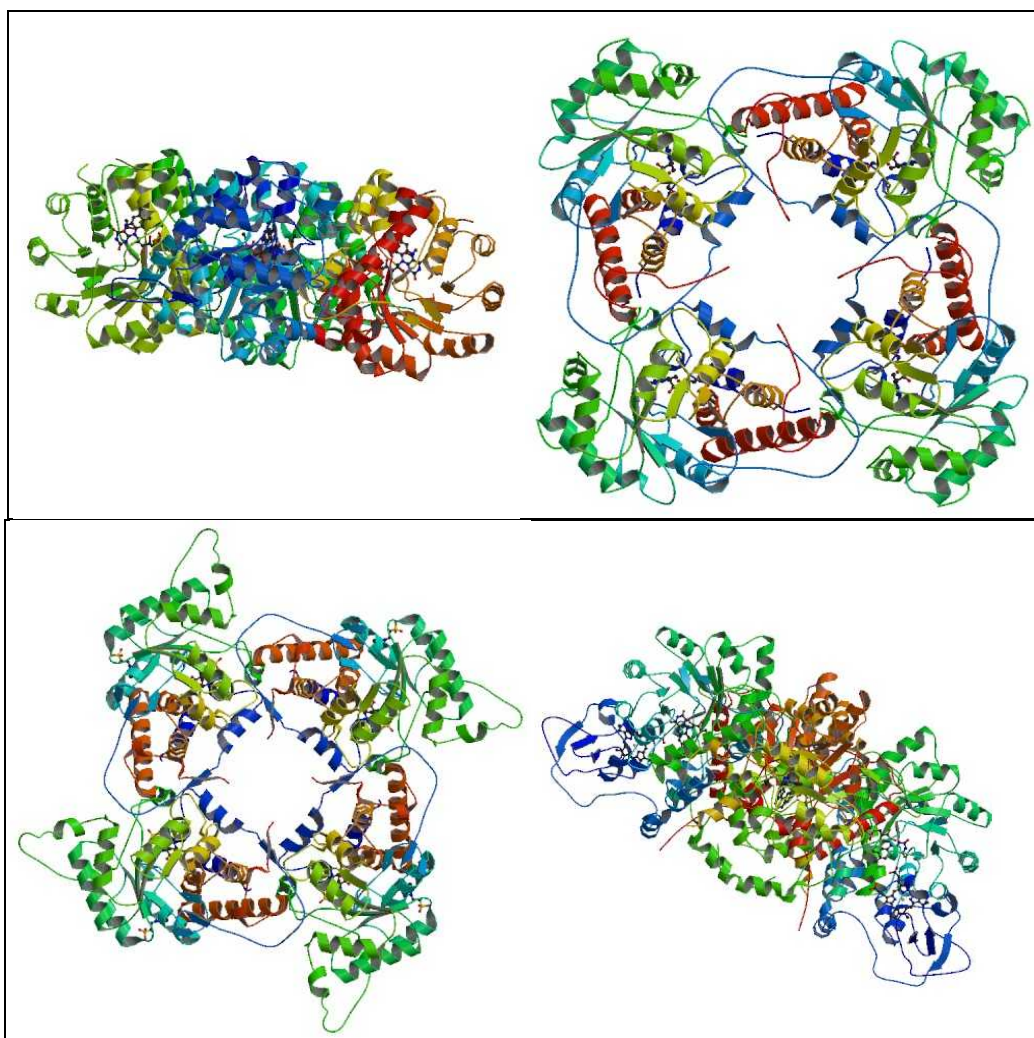
Figure 2: Structures of the members of flavoproteins. From top left to bottom right: HAO, GLO, MDH, B2. in all structures the typicall α/β barrel and the binding sites for FMN cofactor can be seen. The C-terminal regions and αC helices are gathered into the center of the tetramer. The barrel of the monomer is inclined by about 45° to the non-crystallographic axis. On the backside of the tetramer, the N-terminal flexible regions and αA, αB helices are located and form a depression.

The LOX tetramer is associated with 1110 water molecules, where 904 of them are located inside the enzyme. Two water molecules are directly located in the active side of each monomer. It was found out that with absence of L-lactate, the active side is occupied by these water molecules.

Critical amino acids for the mechanism of catalysis are Arg268, His265, and Tyr40. Although, the active side of LOX includes space L-lactate on the FMN plane, whereas GLO is just able to house glycolate. Lactate differs from glycolate only by the presence

of an additional methyl group, but in terms of dipole moment and occupancy of space around the FMN group they have more differences. FMN surrounding residues are at least Y40, Y146, and H265, where two of these are also critical for mechanism as described above. As the geometrical arrangement of the three surrounding residues provide compelling evidence for the location of the L-lactate substrate, Y215 and L211 are located in the flexible region among four monomers and may perform a plausible combination to recognize the substrate. The three Tyr residues as well as H265 and L211 seem to function synergistically to determine the chirality of the substrate, which in fact is not given within the GLO.

In the GLO as well as in mandelate oxidase (MDH; PDB code 1p4c), long-chain hydroxyL-acid oxidase (HAO; PDB code 1tb3) and flavocytochrom B2 (B2; PDB code 1fcb), which are all members of the flavoprotein family (Figure 2), the substrate-binding region is well conserved [Leiros et al., 2006].

The crystal structure of GLO and flavocytrochrome b_2 also show that in both cases at position 99 an alanine is present (Figure 3), which is not the case in Lactate monoxygenase (LMO), where a glycine residue is located [Umena et al., 1977]. The alanine in GLO and flavocytochrome b_2 is in close contact with the flavin N-5-position on the re-face of the flavin [Yorita et al., 1996]. The smaller glycine residue seems to allow the keto acid product to remain bound to the reduced enzyme sufficiently long that decarboxylation can occur and the ternary complex of oxidized flavin, pyruvate and hydrogen peroxide is formed.
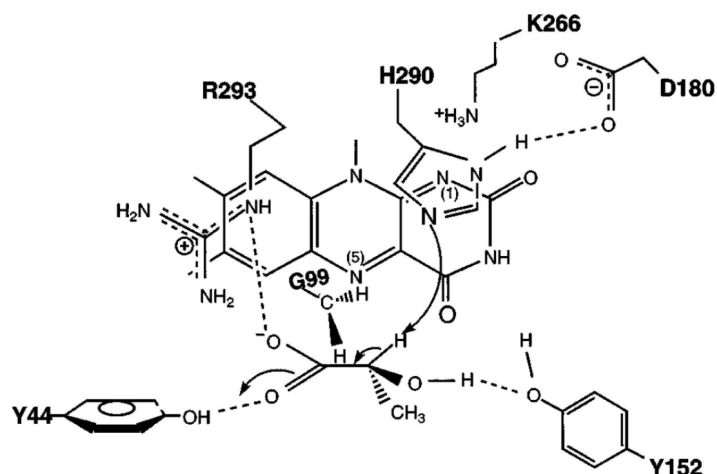
Figure 3: Active site of LOX based on the structure of glycolat oxidase and flavocytochrome b$_2$.

To proof this hypothesis glycine 99 of the L-lactate monoxygenase was changed to alanine [Sun et al., 1996] and the homologues position in LOX, position 95, was point mutated to glycine [Yorita et al., 1996]. Results showed that the LMO G99A acts as a LOX. However, oxygen reactivity is much lower compared to a true LOX [Leiros et al., 2006].

In LOX A95G the reaction pathway is not changed as suspected. Nevertheless, affinity and reactivity of small molecules changed remarkably and the dissociation constant for L-lactate was increased 8-fold. The change of a methyl group with a hydrogen in A95G LOX leads to a 2-fold higher turnover number with DL-α-hydroxy-n-butyric acid compared to L-lactic acid. Also DL-α-hydroxy-n-valeric acid, DL-glyceric acid, and L-mandelic acid are relatively high concerning turnover numbers compared to those of the wild type LOX [Yorita et al., 1996].

## 1.2.	Deracemisation and dynamic kinetic resolution

Most of the important physiological compounds occurring in nature and produced chemically are chiral. Enantiomeric pure amino acids, hydroxy acids and sugars are widely used in the fine chemical and pharmaceutical industry. Therefore the synthesis of those compounds via cost-effective methods has become an important goal. It is possible in some cases but generally very difficult, and in particular a large-scale production is extremely problematical [Soda et al., 2001]. Chiral compounds are usually produced by growing, intact, resting, and dried cells, and enzymes in either dynamic kinetic resolution (DKR) or deracemisation of racemic chiral compounds [Oikawa et al., 2001]. Therefore, attention has turned to the development of asymmetric processes, in which either racemic mixtures are converted to enantiomerically pure compounds or achiral starting materials are converted to chiral non-racemic products [Turner et al., 2004]. Special interest in the DKR of secondary alcohols by combining enantioselective lipases with transition-metal-based racemization catalysts has evolved recently. It was shown that (S)-and (R)-configured alcohols can be prepared by the use of a commercially available (S)-selective subtilisin from *Bacillus licheniformis* as the enantioselective acylation catalyst [Kim et al., 2003]. It was also found, that pre-treating of the subtilisin with a non-ionic surfactant leads to an approximately 4000-fold increase of activity of the biocatalyst [Pamies et al., 2003]. Alternatively to metal-based racemization catalysts, it was shown that acid zeolites are also efficient heterogeneous catalysts for alcohol racemization [Wuyts et al., 2003]. However, a more attractive option of racemization is the use of enzymes instead of metal catalysts because of milder reaction conditions [Schnell et al., 2003]. In fact, the DKR using transition metal complexes is a well established method. Further developmentof a greater range of substrates and a higher importance with respect to S-configured alcohols, the DKR will be a method of high interest in the future [Turner et al., 2004]. 2-hydroxy acids are studied very intensively in organic chemistry, stereochemistry, and biochemistry with the background that these acids are important metabolites in various organisms. Lactate is one of those 2-hydroxy acids where in the past several methods for production of the enantiomer have been developed [Oikawa et al., 2001]. However, D-lactate is much

more difficult to produce than the L-configuration, though D-lactate is more useful as a starting material for the synthesis of agrochemicals, angiotensin-converting enzyme inhibitors and others. The production of D-lactate usually is done by fermentation with *Lactobacillus delbrueckii* and several other lactic acid bacteria [Streitenberger et al., 2001]. A recent development of the one-pot chemo-enzymatic method for the deracemisation of D-enantiomerization of DL-lactate was established by the group of Oikawa [Oikawa et al., 2001]. Here, LOX from *Aerococcus viridans* was used in order to selectively oxidize L-lactate to pyruvate. Pyruvate is then reduced again to racemic lactate with sodium borohydrid (Figure 4).
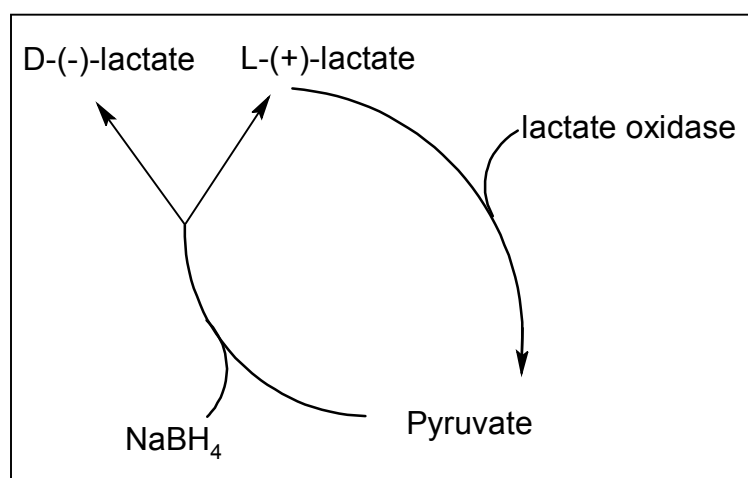
Figure 4: One-pot chemo-enzymatic deracemization of DL-lactate catalysed by LOX from *Aerococcus viridans*.

With optimized reaction conditions the highest yield is obtained at pH 8.0 and 8.5 with a temperature of 37°C. It was also found that sodium borohydride was much more effective than sodium cyano borohydride as the reducing agent. However, a larger amount of sodium borohydride than 0.05mg/mL decreased the final yield. L-lacate was converted to D-lactate and pyruvate, but it was shown that that the amount of sodium borohydride was insufficient to reduce pyruvate formed in the early stage of reaction. However, sodium borohydride disappears after an incubation of about 70 min. Nevertheless, the theoretical yield of D-lactate was gained after 70 min as well.

DL- lactate in the reaction mixture did not affect the yield and was fully converted to the D-enantiomer. Even if a multiple of concentration of the racemic mixture is used, though a multiple of time for the conversion was required [Soda et al., 2001].

2. Material and Methods

2.1. Expression of *Av*LOX A95G

Expression of *Av*LOX A95G in BL21 (DE3) was done in a pre culture over night containing 0.55% glucose monohydrate, 1% peptone, 0.5% yeast extract, 0.5% NaCl, 1% NH_4C), 0.025% $MgSO_4$ * 7 H_2O, 100μL/L poly(propylene glycol), 0.3% K_2HPO_4, 0.6% KH_2PO_4, $0.2*10^{-3}$% thiamine, 0.0115% ampicillin, $0.4*10^{-3}$% $FeSO_4$ * $7H_2O$, $0.1*10^{-3}$% $MnSO_4$ * H_2O, $0.04*10^{-3}$% $CuSO_4*5$ H_2O, $0.01\%*10^{-3}$% H_3BO_3, $0.02*10^{-3}$% $ZnSO_4$ * 7 H_2O, $0.02*10^{-3}$% Na_2MoO_4*2 H_2O and $0.04*10^{-3}$% $FeCl_3$. The optical density (OD_{600}) of the pre-culture, grown over night at 37°C, had a value of about 5. The main culture (same ingredients as or the pre culture except a 4 fold higher amount of glucose) was inoculated to an OD_{600} of 0.5 directly to the fermenter. Temperature, pH, stirring and oxygen partial pressure in the B.Braun Biotech International Biostat®C, Type CT5-2 fermenter were controlled and adjusted automatically during fermentation. The pH was balanced before start at pH 7.0 and pH 4 with a ready-to-use calibration solution.. The pO2 was fixed to a minimum of 40%. Temperature was set to 37°C before induction and then reduced to 30°C. Induction took place with 5mL of isopropyl β-D-1-thiogalactopyranoside (IPTG) with a concentration of 250μg/mL, which was a 1000-fold stock solution at an OD_{600} of 2.4. 50mg/mL Amp was added as well with the IPTG. Concurrent with the induction of the biomass the glucose level was measured continuously over time to determine the endpoint of fermentation with glucose stripes (Diabur Test 5000, Roche Diagnostics). OD_{600} was measured during the whole process of fermentation with Beckman Coulter Photometer. After the whole consumption of glucose the fermentation was stopped and the biomass was centrifuged for 20 minutes at 6000 rounds per minute (rpm) in a Sorvall centrifuge.

2.2.   Purification

Precipitation

Removal of precipitated protein at a concentration of 1.5 M $(NH_4)_2SO_4$

Hydrophobic Interaction Chromatography (HIC)

Phenyl-Sepharose FF (High Sub) column conditions:

CV 64 mL

Maximum flow: 6 mL/min

Binding buffer: 50 mM potassium phosphate buffer containing 1.5 M ammonium sulfate, pH 7.0

Elution buffer: 50 mM potassium phosphate buffer, pH 7.0

Maximum pressure: 5 bar

Maximum sample load: 100 mg protein

Desalting

Removal of salt by replacing the buffer containing (NH4)2SO4 by 50 mM potassium phosphate buffer, pH 7.0 through repeated cycles (more than 4) of concentration to less than 10% volume and dilution using Vivaspin 20 ultrafiltration tubes.

Ion Exchange Chromatography (MonoQ)

Mono Q column conditions

CV: 1mL

Maximum flow: 3 mL/min

Binding buffer: 50 mM potassium phosphate buffer, pH 7.0

Elution buffer: 50mM potassium phosphate buffer containing 1M potassium chloride, pH 7.0

Maximum pressure: 40 bar

Maximum sample load: 45 mg protein

After centrifugation of the biomass French pressing to disrupt the cells was performed. A following ultra-centrifugation of the disrupted cells at 30.000 rpm for 45 minutes (min), the pellets were re-suspended in approximately 20mL of a 50mM phosphate buffer (PO_4 buffer) with a pH 7.0. This solution was used for further purification. All buffers used were filtered and degassed.

2.2.1. Ammoniumsulfate precipitation

For the ammonium sulfate precipitation the cell suspension in 50mM PO4-buffer was used ($(NH_4)_2SO_4$. To precipitate the *Escherichia Coli* (*E. coli)* proteins in solution ammonium sulfate was added to an end concentration of 1.5 M. The crude extract was kept on ice where a stock-solution of 3.5 M ammonium sulfate was added drop-wise during slow mixing of the solution with a stirring rod. After precipitation the solution was left on ice with continuous stirring for 30 min. To get rid of the precipitated proteins the solution was centrifuged in a falcon tube at 13.000 rpm for 30 min in the centrifuge. The supernatant was carefully removed into a Vivaspin tube and concentrated for further processing. The pellet was discarded.

2.2.2. Hydrophobic interaction chromatography

For the Hydrophobic interaction chromatography (HIC) a "High Trap Phenyl FF (low sub)" was used. The column volume was 64mL with a maximum flow of 13 mL/min and a maximum pressure of 0.5 MPa (70 psi or 5 bar). The maximum load onto the column was 100 mg of protein. Binding buffer was a 50 mM potassium *di*-hydrogen phosphate (KH_2PO_4) buffer containing 1.5 M $(NH_4)_2SO_4$. Elution buffer was a KH_2PO_4 buffer with a concentration of 50 mM. There was no further sample preparation necessary because the protein has to be in a 50 mM PO_4 buffer with 1.5 M $(NH_4)_2SO_4$, which was the case because of the $(NH_4)_2SO_4$ precipitation described above. The purification was performed on an Äkta FPLC instrument (Amersham Bioscience) at room temperature (RT).

To guarantee a good performing of the column a Cleaning in Place (CIP) was done which consists of 1 CV of water (H_2O), followed by 1CV of 0.5M sodium hydroxide (NaOH) and 2 CVs of H_2O. The column was stored in 20% ethanol (98% purity) at 4°C.

2.2.3. Desalting of protein

For further processing of the HIC purified enzyme it had to be desalted. Two possibilities were tried. On the one hand, a concentration and diluting procedure with Viva-spin tubes was done. The enzyme was concentrated and afterwards refilled with buffer (KH_2PO_4, 50mM pH 7.0) to 20 mL. This process was repeated three times. With the fourth refilling up to 5 mL the desalting was finished. On the other hand, Nap®-columns were used. Nap®- columns are size exclusion columns where the small salt molecules are washed out faster than the enzyme molecules. The columns are equilibrated with the buffer (KH_2PO_4, 50mM pH 7.0). After loading of the protein in a certain volume a certain amount of buffer had to be added to elute the protein. Note, that the volume of equilibration, protein loading and elution depend on the size of the Nap-column used. Protein containing fractions where collected. The other fractions were discarded.

2.2.4. Ion exchange chromatography- MonoQ

The desalted protein preparation was further purified by strong ion exchange chromatography (MonoQ). The column had a volume of 1mL. A maximum flow rate of 0.5-3 mL/min was allowed. Pressure should not exceed 4MPa (580 psi; 40bar). Loading capacity was 45 mg of total protein in the sample. The binding buffer was a 50mM KH2PO4 buffer, pH 7.0. Elution buffer was the same except the addition of 1.5 M potassium chloride (KCl). The purification was done with the Äkta FPLC instrument at RT.

2.3.   Kinetics

2.3.1. Volumetric Activity

The activity was measured with a coupled enzymatic assay (Figure 5) using two enzymes, the LOX and the horseradish peroxidase (POD) to detect L-Lactatic acid. 5-10μL of LOX A95G enzyme appropriately diluted in 50 mM potassium phosphate buffer was added to the activity assay containing 40 mM 3,3-Dimethylglutaric acid (DMGA),2.5 units peroxidase, 1.5 mM 4-aminoantipyrine (AAP), 50mM L-lactic acid and 0.04% (volume/volume; v/v) N,N- Dimethylaniline in a total volume of 0.5 mL reaction mixture at pH 6.5.
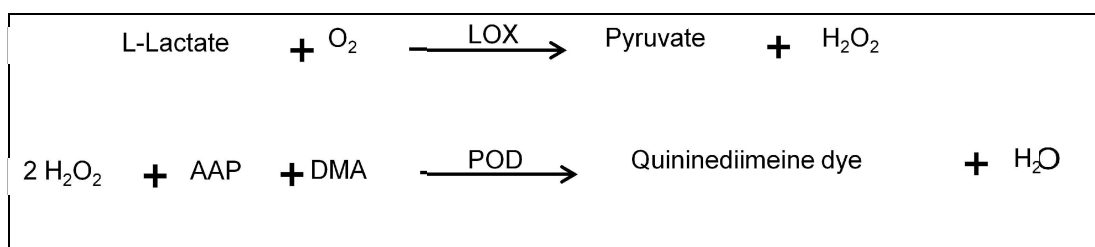
Figure 5: Activity measurement with a coupled assay. The two-enzymatic assay is using LOX in the first step to generate H$_2$O$_2$ which is then further converted to Quinonediimine by the second enzyme, horseradish peroxidase.

The reaction took place in an eppendorf tube in the thermomixer at 37°C. After 10-20 minutes the reaction was stopped by addition of Dodecylbenzenesulfonic acid (DBS; 0.25%). The color development is measured at 565 nm in a Beckmann Photometer using a plastic cuvette with a light path of 1 cm. The absorbtion of the endpoint measurement should neither exceed 0.8 nor fall below a value of 0.1. In the table below more details on concentration and preparation of each solutions used in the assay is given.

The volumetric activity (U/mL) of the enzyme was calculated using the following equation.

$$Vol.\ activity\ [U/mL] = \frac{Abs * 1.51\ [mL] * fv}{35.33\ [mM] * 0.5 * t\ [min] * Vol\ [mL]}$$

U/mL…………Volumetric activity, where Unit per definition means µmol/min

Abs………….Absorption value measured in the photometer

1.51…….......total volume of the assay [mL]

fv…………….dilution factor

35.33………..extinction coefficient of quinonediimine at 565nm [mM]

0.5…………..Conversion factor based on one mol of H_2O_2 produces half a mole of quinonediimine dye

t……………..Time [min] per unit definition

Vol………......volume of used enzyme [mL]

2.3.2. Protein concentration

Protein concentration was determined with Rotiquant® , which basically is the method of Bradford. This assay is a dye-binding assay in which a differential colour change of the dye gives the protein concentration of the specimen. Therefore standard-solutions with a defined concentration are prepared before performing the analytical test. Here Bovine serum albumin (BSA) was used as standard from 0-1 mg/mL. The samples had to be diluted into this range. 1mL of reagent was added to 20µL of sample. Short agitation ensured a proper mixing of the solution. After 20 minutes incubation at RT the absorption was measured at 600 nm with a Beckmann Coulter photometer using plastic cuvettes with 1 cm path length.

2.3.3. Michaelis-Menten Constant (KM) determination

For determination of the K_M value of the A95G mutant enzyme the substrate was prepared in different concentrations from 0 – 500mM. The measurement was done with the activity assay described above. A master mix was prepared, which contained all ingredients except the substrate, and sampled into the cuvettes. Further the substrate was added in the different concentrations. Measurement was done as described above. To calculate the K_M value a hyperbolic curve was fitted to the points which use equation 2.

$$v = \frac{c[P]}{dt} = \frac{vmax * [S]}{KM + [S]}$$

Equation 2

2.3.4. Stability determination

Determination of stability was done in eppendorf tubes in the thermomixer at 37°C without shaking. Therefore a defined enzyme preparation of about 0.02 mg/mL in a 40mM HEPES buffer, containing 150 mM NaCl pH 8.1, was used. Different concentrations of carbonate (0-500 mM) were added to the samples. After certain time points, activity was determined with the oxidase assay described in chapter 2.3.1 The specific activity was calculated according to Equation 3.

$$U/mg = \frac{Vol.\, activity\, [U/mL]}{Protein\, concentration\, [mg/mL]}$$

Equation 3

The residual activity was calculated according to equation 4.

$$Residual\,activity = \frac{Specific\,activity\,of\,measured\,value\,[U/mg]}{Specific\,activity\,of\,sample\,at\,t\,(zero)\,[U/mg]}$$

<div align="right">**Equation 4**</div>

Data were fitted with an exponential function and an intersection of 1. The equation, y= e $^{-kx}$ was used. y is activity, x is time, and k is the constant of decay and the positive value was further used to determine the half-life time of the enzyme (Equation 5).

$$t\frac{1}{2} = \frac{LN(2)}{k}$$

<div align="right">**Equation 5**</div>

The values of half-life time were plotted in a bar chart for further comparison.

2.4. One-pot chemo-enzymatic de-racemization

2.4.1. Small scale reaction

The small scale experiment was preliminary to find out the right conditions for the large scale experiments. It was done in a 1.5 mL eppendorf tube in the thermomixer at 37°C. Shaking was defined at 600 rpm. The lid of the tube was open during the whole experiment to guarantee oxygen supply. Note, that it was just surface air without any extra gassing. The mutant enzyme A95G was diluted to a defined concentration in 20 mM 2-Amino-2-hydroxymethyl-propane-1,3-diol (Tris), pH 8.0. The substrate DL-mandelic acid was also prepared in 20 mM Tris buffer and the pH was adjusted to 8.0. Enzyme, substrate and buffer solution were mixed together and incubated at 37°C. For reduction of the intermediate PGA to the racemic mandelic acid, $NaBH_4$ is added. Samples were taken after several time points.

2.4.2. Large scale reaction

The large scale reaction was done in a 30 mL glass reactor with a jacket to temper. The reactor was placed on a stirring plate. Stirring happened with a stirring rod at 300 rpm. Temperature was kept constant at 37°C through a water bath with a temperature control unit. A pH electrode was mounted and enabled continuous measurement to guarantee a pH of 7.5. Starting conditions were DL-mandelic acid in a certain concentration pre-warmed in the reactor with 1000 U of catalase. The first sample was taken under this conditions. By addition of the enzyme (1 U/mL) the reaction was started. After one hour $NaBH_4$ (1U/mL) was added. The addition of $NaBH_4$ led to a pH-change and pH had to be adjusted. After 10 – 15 minutes of reaction time for NaBH4 fresh enzyme (1 U/mL) was added to the cycle again. The whole procedure was repeated for 5 cycles to guarantee a complete de-racemization of mandelic acid.

2.5.　　High pressure liquid chromatography analysis

High pressure liquid chromatography (HPLC) was done on an FPLC Agilent system. For chiral separation a Chiralpak ® column and a Chirobiotic R ® was used in reverse phase. For the Chiralpak ® two mobile phases were prepared. Buffer A was 0.1% trifluoroacetat (TFA) in $H_2O$and buffer B, which served as eluent, was 0.1% TFA in acetonitrile. A gradient to 30% of buffer B within 60 min was conducted. A step of 100% of buffer A for 20 more minutes to equilibrate the column. For the Chirobiotic® the mobile phase consisted of methanol (98% purity) triethylamin and acetic acid in a ratio of 100:0.4:0.1. Isocratic elution was used and the run was 20- 30 min. Measurement was done with a UV detector.

2.6.   Crystallization

The basic method of crystallization was the hanging drop vaporization (Figure 6). The crystallization was done in 24-well plate where each well contains the reservoir with different conditions of buffer, pH and additives (Table 1). The protein drop was put onto the cover slide in a certain concentration mixed with reservoir. To make the well dense and avoid vaporization, oil was put onto the wall of the well and the cover slide was put onto the ring of oil.
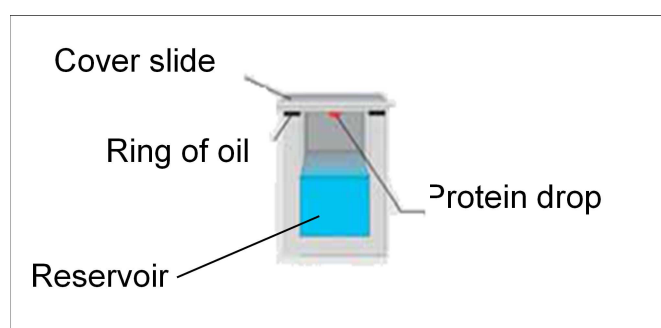
Figure 6: schematic assembling of hanging drop method for crystallization. The work was done in a 24-well plate, each covered with its own cover slide and the single drop hanging into the well with the reservoir filled.

The 24-well plate was stored in a special room where temperature (25°C) and humidity were controlled.

Table 1: Different conditions of preparing crystals in the 24-well plate. The red highlighted condition was the crystal harvested and measured at the Synchrotron.

50mM Tris pH	PEG 3350 [%]	Pyruvat [M]	A95G 10mg/mL [μL]	Reservoir [μL]
8	20%	0,1	1	1
8	20,2	0,1	1	1
8	20,4	0,1	1	1
8	20,6	0,1	1	1
8	20,8	0,1	1	1
8	30	0,1	1	1
8	32	0,1	1	1
7,53	20	0,1	1	1
7,53	22	0,1	1	1
7,53	24	0,1	1	1
7,53	28	0,1	1	1

7,53	32	0,1	1	1
7,02	20	0,1	1	1
7,02	24	0,1	1	1
7,02	28	0,1	1	1
7,02	32	0,1	1	1
8	32	0,1	2	1
7,53	32	0,1	2	1
8	34	0,05	1	1
7,53	34	0,05	1	1
7,5	30	0,1	1	1
8	30	0,1	1	1
8,5	30	0,1	1	1
7,5	35	0,1	1	1
8	35	0,1	1	1
8,5	35	0,1	1	1
7,5	40	0,1	1	1
8	40	0,1	1	1
8,5	40	0,1	1	1
7,5	45	0,1	1	1
8	45	0,1	1	1
8,5	45	0,1	1	1
7,5	30	0,05	1	1
8	**30**	**0,05**	**1**	**1**
8,5	30	0,05	1	1
7,5	35	0,05	1	1
8	35	0,05	1	1
8,5	35	0,05	1	1
7,5	40	0,05	1	1
8	40	0,05	1	1
8,5	40	0,05	1	1
7,5	45	0,05	1	1
8	45	0,05	1	1
8,5	45	0,05	1	1
7,5	47,5	0,05	1	1
8	47,5	0,05	1	1
8,5	47,5	0,05	1	1
7,44	30	0,1	1	1
7,64	30	0,1	1	1
7,86	30	0,1	1	1
7,44	31	0,1	1	1
7,64	31	0,1	1	1
7,86	31	0,1	1	1
7,44	32	0,1	1	1
7,64	32	0,1	1	1
7,86	32	0,1	1	1
7,44	33	0,1	1	1
7,64	33	0,1	1	1
7,86	33	0,1	1	1
7,44	34	0,1	1	1

7,64	34	0,1	1	1
7,86	34	0,1	1	1
7,44	35	0,1	1	1
7,64	35	0,1	1	1
7,84	35	0,1	1	1
7,44	30	0,05	1	1
7,64	30	0,05	1	1
7,86	30	0,05	1	1
7,44	31	0,05	1	1
7,64	31	0,05	1	1
7,86	31	0,05	1	1
7,44	32	0,05	1	1
7,64	32	0,05	1	1
7,86	32	0,05	1	1
7,44	33	0,05	1	1
7,64	33	0,05	1	1
7,86	33	0,05	1	1
7,44	34	0,05	1	1
7,64	34	0,05	1	1
7,86	34	0,05	1	1
7,44	35	0,05	1	1
7,64	35	0,05	1	1
7,84	35	0,05	1	1
7,44	30	0,03	1	1
7,64	30	0,03	1	1
7,86	30	0,03	1	1
7,44	31	0,03	1	1
7,64	31	0,03	1	1
7,86	31	0,03	1	1
7,44	32	0,03	1	1
7,64	32	0,03	1	1
7,86	32	0,03	1	1

The growing of crystals was controlled periodically. If a crystal had a certain size and was single grown (Figure 7) it was harvested. The harvesting was done with a mounting nylon loop where the crystal was taken out of the well and put into a cryoprotectant solution, which contain reservoir solution (90%) with 10% ethylenglycol. The single crystal was mounted again with the nylon loop and flash-cooled in liquid nitrogen.The x-ray measurement was kindly done by Prof. Dave Wilson at the Stanford Synchrotron Radiation Lab, Beamline 7-1 on 29 June 2011. Data were reduced using the HKL2000 program suite.

Figure 7: Single grown crystal from A95G.

2.7.   Structure refinement

Molecular replacement [Collaborative Computational, 1994] to determine rotation and translation using the WT structure of LOX (PDB entry 2DU2) was used with the program ccp4i. Refinement using REFMAC5 program by the maximum-likelyhood method [Murshoduv et al., 1997] was used to get a final R of 17.6% and Rfree of 21.2%. Water molecules were picked from different Fourier electron density maps. PROCHECK analysis was also done with ccp4i. WinCoot 07-pre 1 software [Emsley et al., 2010] was used as structur illustration during refinement. Pymol Viewer was used for illustration.

3. Results & Discussion

3.1.   Cultivation

The cultivation in the Biostat® C fermenter was successfull in production of biomass and protein in crude extract. In comparison to cultivation in shaking flasks, which method is not described here, the concentration of the enzyme of interest was increased. In the figure below, one can see the growth curve of the *Av*LOX A95G over the nearly 9 hours of fermentation time.
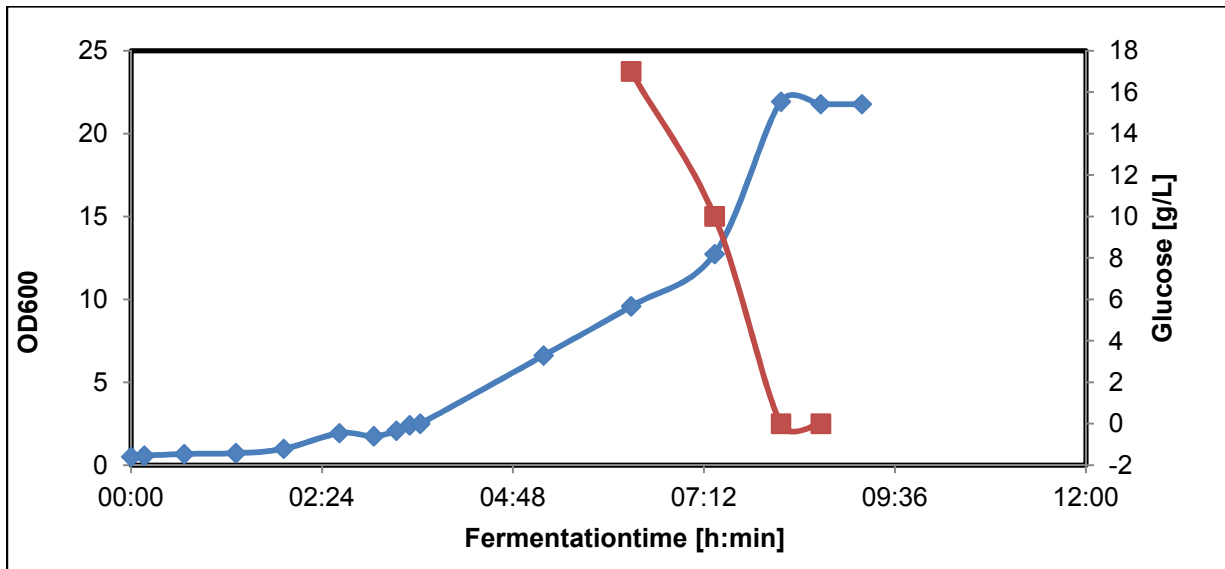
Figure 8: Determination of optical density (blue line) and glucose consumption (red line) of AvLOX A95G during fermentation in the Biostat C over time.

The blue curve in figure 8 shows the OD at 600nm measured over the time. Reaching an OD of approximately 2.5, induction with IPTG was done which can be seen after 3.5 hours after inoculation. After induction also the glucose level was determined over time, indicated as red line in the figure above (Figure 8). After the consumption of glucose the fermentation was stopped. Exact values of OD 600 and glucose can be observed in the table below (Table 2).

Table 2: Values of optical density and glucose measured during fermentation.

Ferm.time [h:min]	OD measured	fv	OD 600	Glucose level [g/L]
00:00	0,500	1	0,500	nd
00:10	0,572	1	0,572	nd
00:40	0,672	1	0,672	nd
01:19	0,726	1	0,726	nd
01:55	0,9826	1	0,983	nd
02:37	0,193	10	1,929	nd
03:03	0,174	10	1,742	nd
03:20	0,207	10	2,073	nd
03:30	0,241	10	2,405	nd
03:38	**Induction with IPTG + Amp**			nd
05:11	0,661	10	6,606	nd
06:17	0,958	10	9,580	17
07:20	1,273	10	12,730	10
08:10	0,219	100	21,920	~ 3,5
08:40	0,218	100	21,770	~ 2
09:11	**End of fermentation**			

A steady control of all parameters gained a higher volume of biomass and increased amount of protein concentration compared to cultivation in shaking flasks. Reasons for that could be the prevention of a pH shift because of acetate produced in *E.Coli*.

3.2.   Purification

3.2.1. Ammonium sulfate precipitation

Ammonium sulfate precipitation was done in two steps as can be read in section materials and methods. After the second precipitation the protein is not pure enough as shown in figure 9. There is a slight accumulation of the protein after precipitation which led to the assumption that there is purification. However, it is not pure enough for measuring the enzyme kinetics. Therefore purification steps had to be added afterwards.
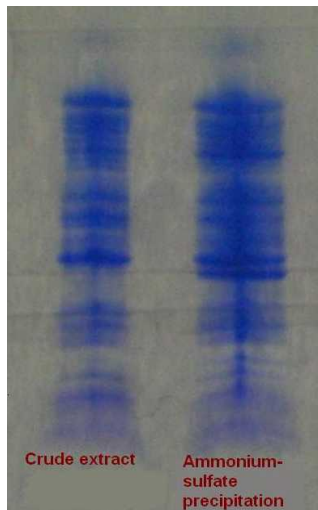
Figure 9: SDS gel of crude extract in comparison to the protein after ammoniumsulfate precipitation. Both protein concentrations are with 1mg/mL of protein on the gel.

3.2.2. Hydrophobic interaction chromatography

In figure 10, one can see an example of HIC purification with a linear gradient of buffer B. The peaks within the first 100 mL were discarded because there is no protein of interest in it. The highest measureable activity is within the fractions 9 to 15. These fractions were measured with the coupled activity assay described previously. There was no measurable activity in all the other fractions. The fractions which show the highest enzyme activity were pooled. To guarantee that the method with the hydrophobic interaction was successful, further schemes (Figure 10) were measured

too. Also within the second purification the activity can be measured within the fractions 9 to 15.
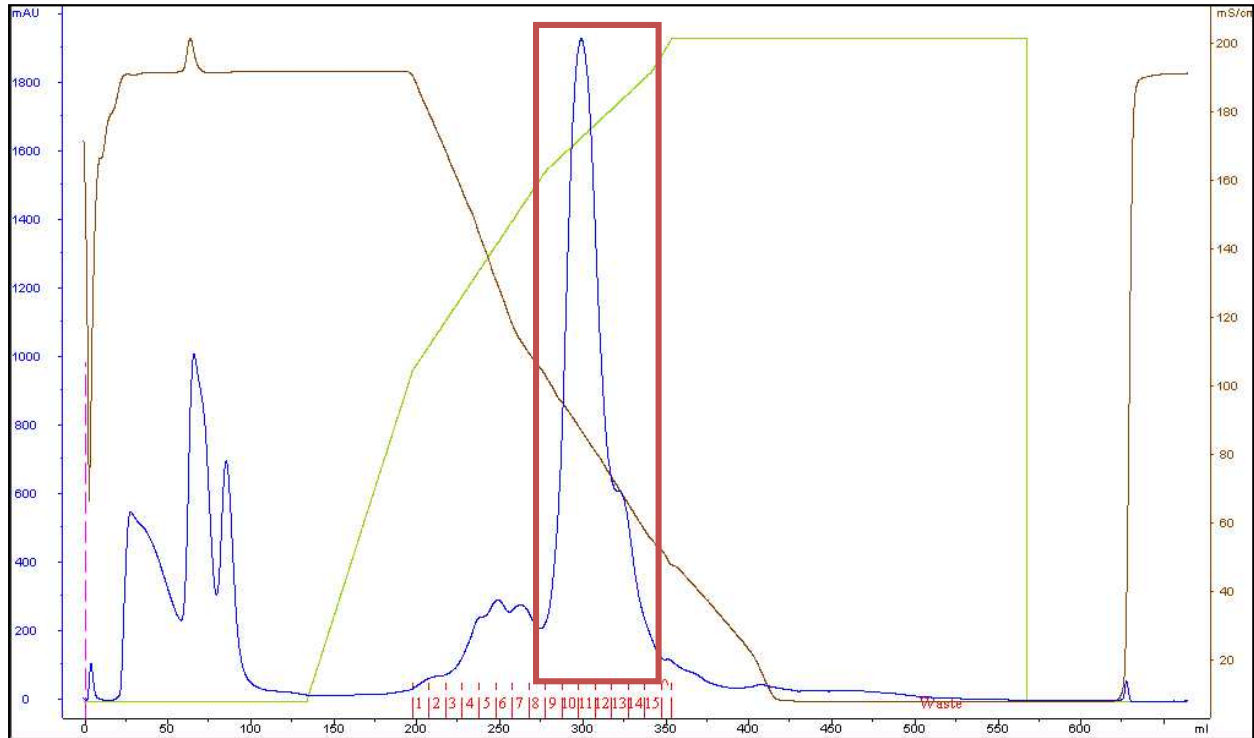
Figure 10: Second scheme of HIC purification with a linear gradient. Here one can see that the program with the linear gradient and the peaks of protein are the same like in figure 9.

The pooled fractions were further put onto a SDS PAGE, seen in figure 11. Here, it can be observed that the protein after HIC purification and a further desalting with Nap® columns do not show any loss of protein. The pooled preparation were separated for the desalting, because of that, one can see two lanes on the gel, which were later on pooled again. The protein preparation in the second line (Wild type preparation from Roche Industries) indicates the purity the protein should have after purification.
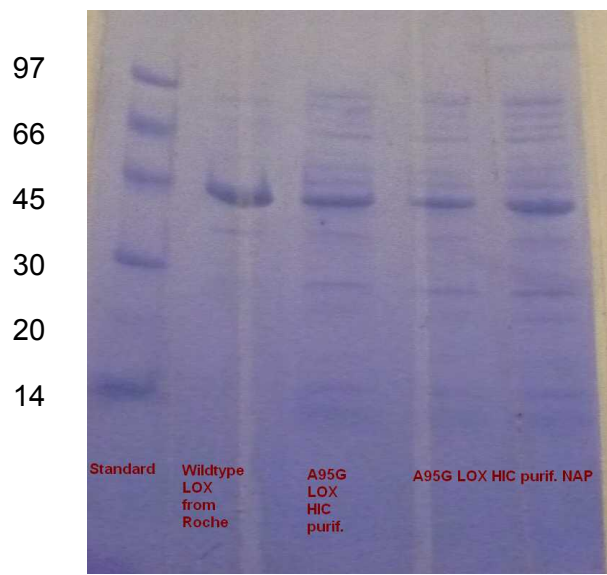
Figure 11: SDS PAGE of A95G after HIC purification and desalting with Nap® columns in comparison with the preparation of Roche which indicates the purity of interest. Standard is a low molecular standard and values are given in kDaltons (kDa).

As there is no highly pure protein, a third purification step was chosen to guarantee that there is no other protein in the preparation.

3.2.3. Ion exchange chromatography- MonoQ

The desalted protein preparation out of HIC purification were loaded onto the MonoQ column and eluted with a stepwise increasing of chloride anion concentration administered from a 50 mM phosphate buffer containing 1 M KCl at a pH of 7.0. An example for the MonoQ purification, which was fully reproducible for the A95G LOX, is shown in figure 12. The SDS Page gel in figure 13 shows the eluted fractions from the last purification step shown in figure 12. The protein is pure and can be used for further measurements.
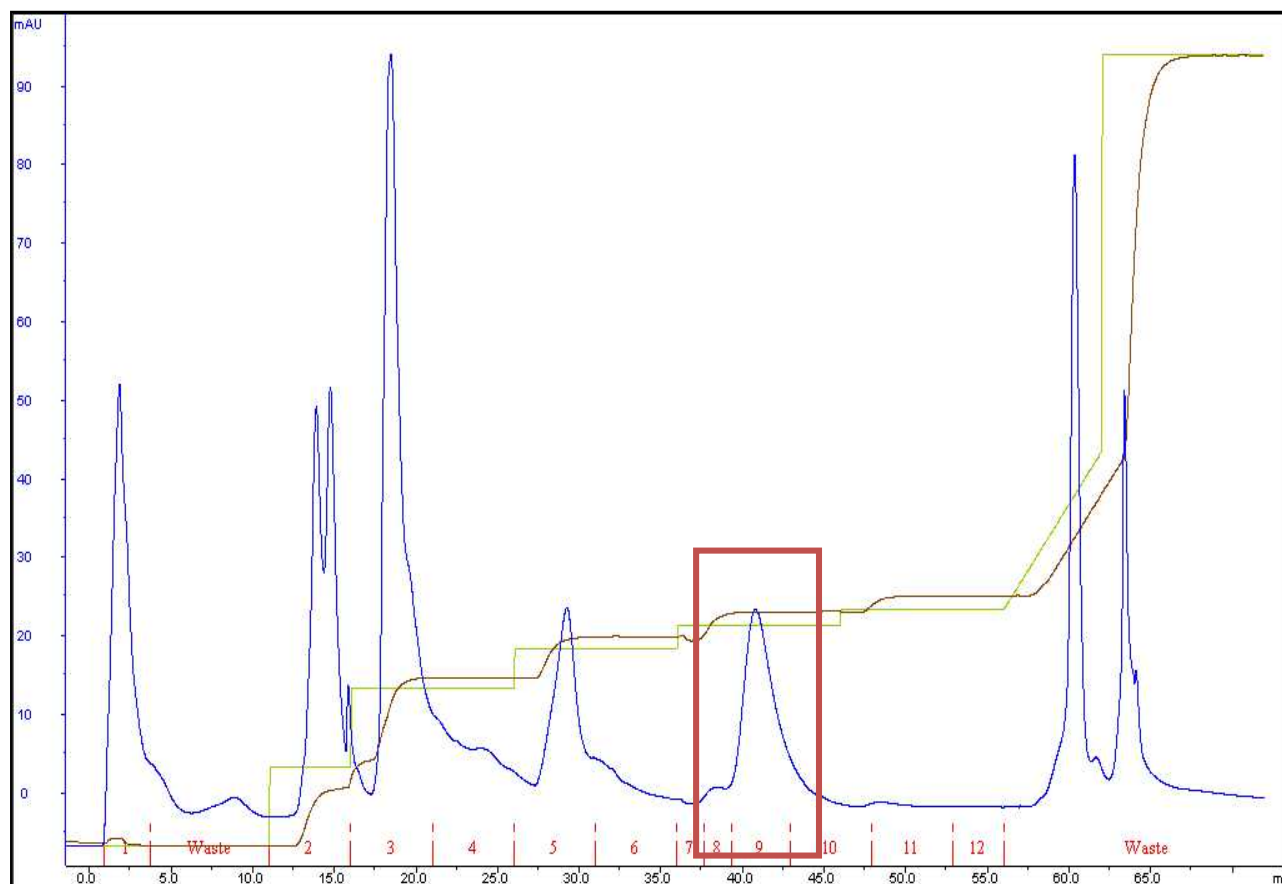
Figure 12: MonoQ purification with step-gradient (green line). The protein elutes at a concentration of about 40%. The UV signal (blue line) in fraction 9 is the protein of interest A95G.

Figure 13: SDS Page gel of MonoQ purification. The lanes in between the two standard (low molecular standard, values given in kDa) lanes on the outer left and right side are from different fractions collected. The fractions in this case are the purifications itself done on different days with the A95G.

3.3.   Characterization

3.3.1. Kinetics

The overall aim of the A95G LOX characterization was to determine the specific activity, where the protein concentration and the volumetric activity are needed. In figure 14 one can observe the standard curve for determination of concentration. The standard protein was BSA in an exact concentration between 0.1 and 0.8 mg/mL. The trend line should be linear and gives the slope. With the R^2 value the accuracy of the line is shown and should not be below 0.98.
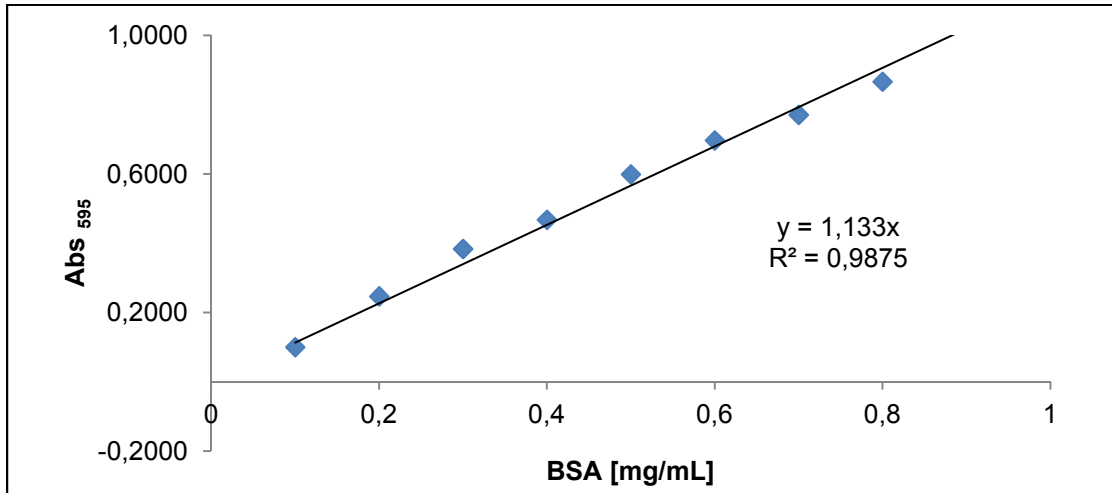
Figure 14: Protein standard curve done with BSA in a range between 0.1 – 0.8 mg/mL.

In table 3 the measurement of the specific activities and the recovery of all steps during purification are listed. All the values are mean values out of at least two independent measurements. The protein was produced in the Biostat C fermenter. The recovery in percent in this table belongs to the total protein in solution. In comparison to other LOX mutants which were cultivated in shaking flasks it shows an increase of final protein.

Table 3: Specific activities and recovery rates of A95G of different steps during purification.

	Specific activity [U/mg]	Recovery [%]
Crude extract	1,8	100,0
after As precipitation	2,1	90,6
HIC	4,5	9,9
MonoQ	17,6	1,7

Possible reasons for these differences in recovery of cultivation in shaking flasks in comparison to the cultivation in the fermenter could be because of the much more stable conditions in the fermenter than in the shaking flasks. Continuous control and regulation of oxygen and pH led to a stable environment for the cells to grow. However, this is not possible within shaking flasks. Here, the temperature is only parameter which can be controlled during growth.

3.3.2. Substrate specificity

Substrate specificity is measured with Michaelis Menten described previously. In figure 15 one can see the graph page of the determination of K_M value of the A95G with L-lactic acid as the substrate.
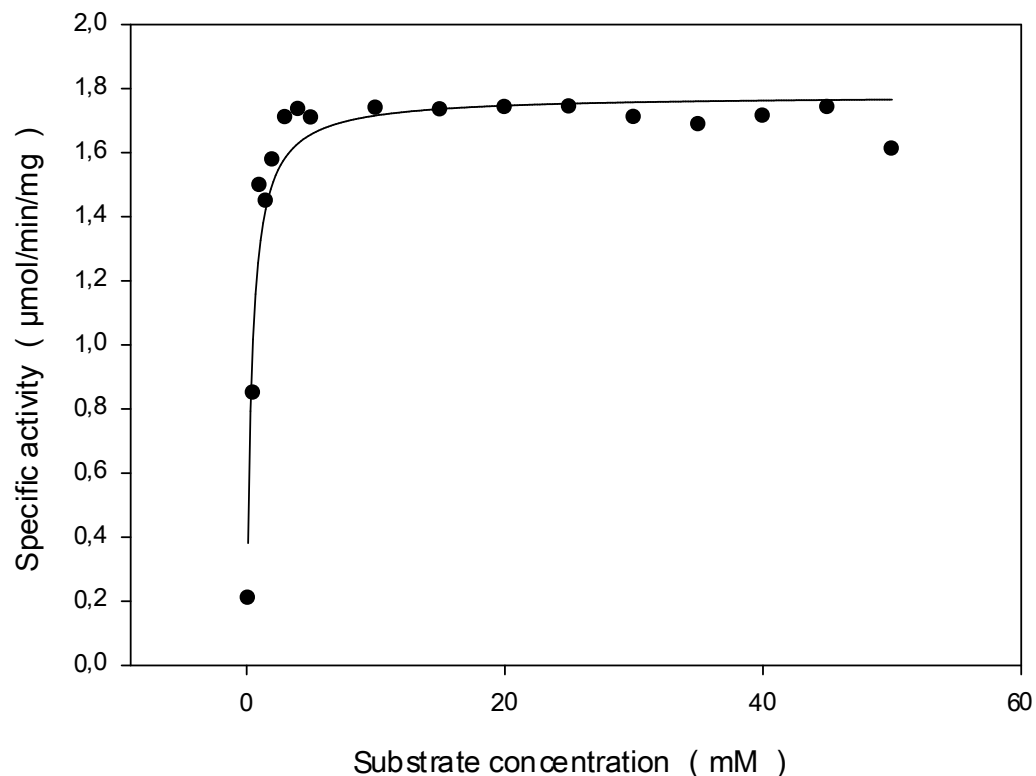
Figure 15: Michaelis Menten curve of A95G with L-lactic acid. The x- axis gives the concentration of substrate, which is present in the cuvette in mM. The y-axis gives the calculated specific activity in µmol/min/mg.

In the table below (Table 4), one can see the substrates measured with the A95G in comparison to the wild type LOX. The L-(+)-lactic acid is the natural substrate of the *Av*LOX wild type and therefore has the highest k_{cat} over K_M value which indicates the enzyme efficiency and is the value of interest for every comparison. In this case the wild type LOX has a nearly 100-fold higher value compared to the mutant. With a closer look at the different substrate it can be assumed that with the most substrates the wild type LOX has a better efficiency than the mutant. However, two of the substrates out of this list show higher efficiency of the mutant than the wild type. L-2-hydroxybutyric acid shows a nearly 20-fold higher efficiency than the wild type. This high number can either be observed because of a large turnover number (k_{cat}) or a small K_M. Nevertheless, both values k_{cat} and K_M of the mutant are multiple folds higher than these of the wild type. The second substrate with a higher efficiency is L-mandelic acid which shows a 4-fold increase. Substrate affinity and turnover number are also increased with this substrate.

Table 4: List of measured substrate with their specific activities, kcat values and KM values.

Substrate		Specific activity [U/mg]	k_{cat} [sec^{-1}]	K_M [mM]	k_{cat}/K_M [mM sec^{-1}]
L-(+)-lactic acid	WT	204.00 ± 1.00	140.00 ± 1.00	0.83 ± 0.03	167.00
	A95G	33.90 ± 1.24	23.20 ± 0.85	12.76 ± 2.84	1.87 ± 0.36
L-glycolic acid	WT	1.40 ± 0.02	0.98 ± 0.01	0.44 ± 0.06	2.20
	A95G	0.83 ± 0.14	0.56 ± 0.14	8.04 ± 0.09	0.70 ± 0.01
L-glyceric acid	WT	1.70	1.16	8.62	0.13
	A95G	0.74 ± 0.10	0.51 ± 0.07	1.27 ± 0.08	0.40 ± 0.03
L-2-hydroxy-3-methylbutyric acid	WT	0.25 ± 0.01	0.18 ± 0.01	3.30 ± 1.30	0.10
	A95G	5.41 ± 2.78	3.70 ± 1.90	32.9337 ± 25.7156	0.1294 ± 0.0599
L-2-hydroxyisocaproic acid	WT	1.60 ± 0.17	1.10 ± 0.12	0.43 ± 0.05	1.00
	A95G	0.33 ± 3.05 *10^{-5}	0.23 ± 2.08*10^{-5}	8.91 ± 1.59	0.03 ± 0.005
L-mandelic acid	WT	0.14 ± n.d	0.10 ± n.d	0.48 ± 0.10	0.2
	A95G	3.28 ± 0.88	2.24 ± 0.60	2.80 ± 0.36	0.80 ± 0.11
L-2-hydroxybutyric acid	WT	2.00 ± 0.02	1.38 ± 0.01	0.43 ± 0.05	1.3
	A95G	48.27 ± 14.95	32.98 ± 10.22	2.04 ± 1.34	18.52 ± 5.42
para-hydroxy mandelic acid	WT	n.d	n.d	n.d	n.d
	A95G	0.07 ± n.d	0.05 ± n.d	6.83 ± n.d	0.01 ± n.d
2-chloro mandelic acid	WT	n.d	n.d	n.d	n.d
	A95G	0.63 ± 0.07	0.43 ± 0.05	0.28 ± 0.09	1.55 ± 0.82
2-fluoro-mandelic acid	WT	n.d	n.d	n.d	n.d
	A95G	5.70 ± n.d	3.89 ± n.d	3.58 ± n.d	1.09 ± n.d
4-fluoro-mandelic acid	WT	n.d	n.d	n.d	n.d
	A95G	1.32 ± n.d	0.90 ± n.d	2.20 ±n.d	0.41 ± n.d
para-methoxy-mandelic acid	WT	n.d	n.d	n.d	n.d
	A95G	1.20 ± 0.07	0.82 ± 0.048	4.66 ± 1.49	0.18 ± 0.048

3.3.3. Stability determination

The stability of A95G measured with addition of carbonate at 50°C can be observed in the table below (Table 5). Here, it can be seen that the enzyme preparation without carbonate in the solution has the highest stability. More than a 60% decrease of stability takes place with addition of 20mM carbonate. However, with a concentration of 50-200mM of carbonate leads to a decrease of stability of about 80%. Within this range the stability stays the same without further loss of stability. At a concentration of 500mM the half-life time of the A95G is at 0.5 days which means a loss of stability of 92%.

Table 5: Half-life times of A95G in presence of different concentrations of carbonate, measured at 50°C. The last row of the table gives the percentage based on the measurement without carbonate and the loss of with addition of carbonate.

	k'	$t_{0,5}$ [days]	%
0mM Carbonat	0,1068	6,490	100.00
20mM Carbonate	0,3018	2,296	35,37
50mM Carbonate	0,4284	1,617	24,92
100mM Carbonate	0,4978	1,392	21,45
200mM Carbonate	0,5273	1,314	20,25
500mM Carbonate	1,2119	0,571	8,80

If the stability is compared with the wild type AvLOX (Figure 16), one can see that with no addition of carbonate the wild type LOX has a nearly 2-fold higher value than the mutant. As mentioned before, with the addition of 20mM carbonate a 2.8-fold decrease in stability of the mutant occurs. Compared to the wild type, one can say that the mutant is more stable because the wild type has a 3-fold decrease with the same concentration. With increasing concentration of carbonate the wild type stability decreases as can be observed in table 7.
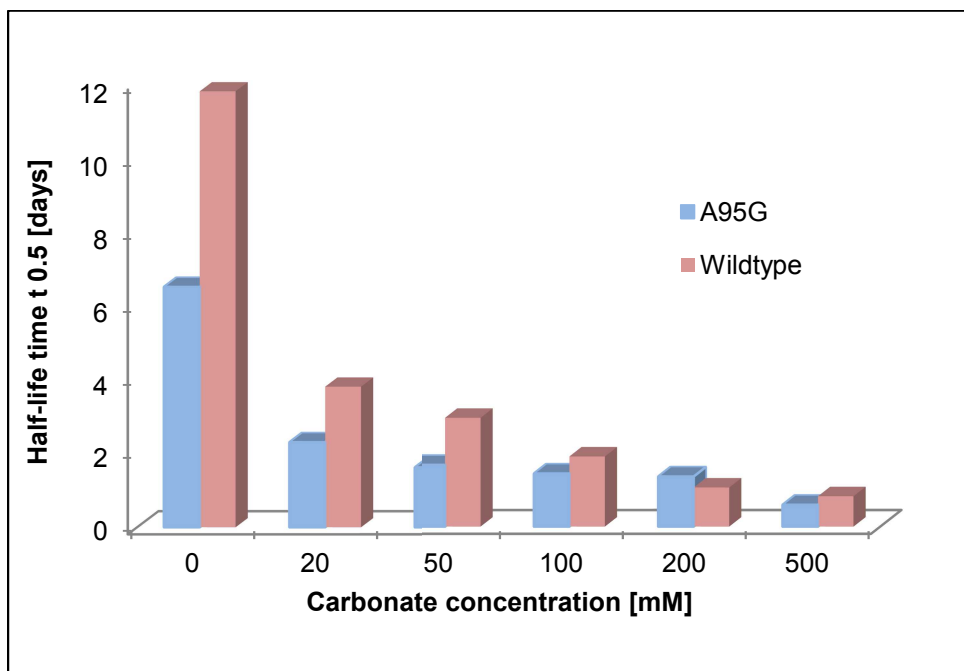
Figure 16: Comparison of stability of A95G and wild type LOX. The red barns represent the wild type of LOX whereas the blue barns represent the mutant. The x-axis shows the concentration of carbonate in mM in the reaction mixture.

Table 6: Stability determination with different concentrations of carbonate in solution of _Av_LOX wild type

	k'	t0,5 [days]	%
0mM Carbonat	0,0589	**11,768**	100
20mM Carbonate	0,1826	3,795	32,25
50mM Carbonate	0,2428	2,854	24,25
100mM Carbonate	0,3766	1,840	15,64
200mM Carbonate	0,6753	1,026	8,72
500mM Carbonate	0,8689	0,797	6,77

The comparison between the wild type and the mutant showed that that the mutant has no increase in stability with or without carbonate.

## 3.4.	De-Racemization

3.4.1. One-pot chemo-enzymatic de-racemization

Analysis and quantification of the D- and the L-mandelic acid was performed by chiral HPLC. The initially used Chiralpak® column was later replaced by a Chirobiotic® column that provided a higher resolution with baseline separation of the analytes. Also a pH change from 8.0 to 7.5 gave a better resolution of the Chirobiotic® column. However, activity of the enzyme did not change with the pH change. For the quantification of D-and L-mandelic acid in the reaction mixtures, standards were measured. For peak identification of the D- and L-mandelic acid the enantiomerically pure compounds were measured (Figure 17). Figure 17 shows UV absorbance traces of the L-mandelic acid in red lines and the D-mandelic acid in blue lines.
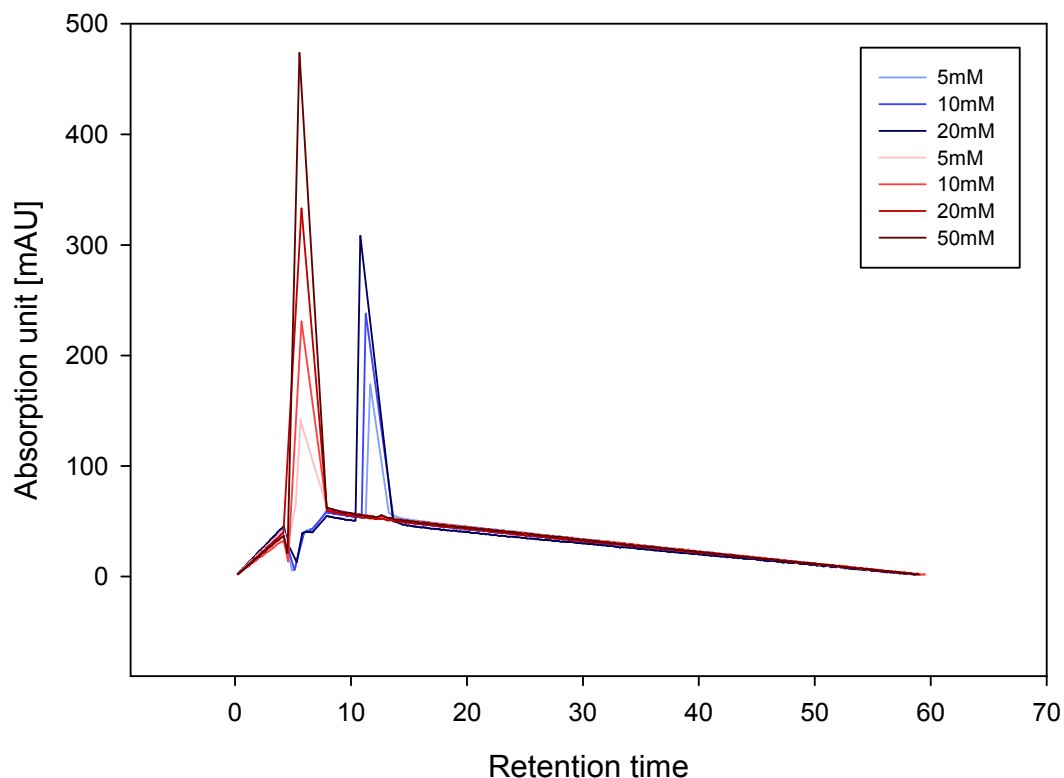
Figure 17: Standards of enantiomerically pure D- and L-mandelic acid in concentrations between 5 and 20mM. The curves in red indicate L-mandelic acid and the blue lines represent D-mandelic acid. The analyte concentration of each curve is given in the inset.

Calibration curves were drawn from peak areas of standards with defined concentrations. Slopes were used to calculate product formation during the one-pot chemo-enzymatic de-racemization from sample peak areas (Figure 18). The areas of the peaks were calculated automatically by the HPLC-software. The intermediate obtained in the reaction was, in accordance with the proposed mechanism, assigned to PGA. Therefore, a calibration curve for phenylglyoxylic acid was recorded by HPLC. However, the phenylglyoxylic acid showed a retention time of about 5 min (figure 19, x-axis) which is close to the retention of L-mandelic acid and causes overlap of corresponding peaks. Therefore, only the concentration of D-mandelic acid in the reaction was used to calculate the kinetic resolution and further the product in the final sample.
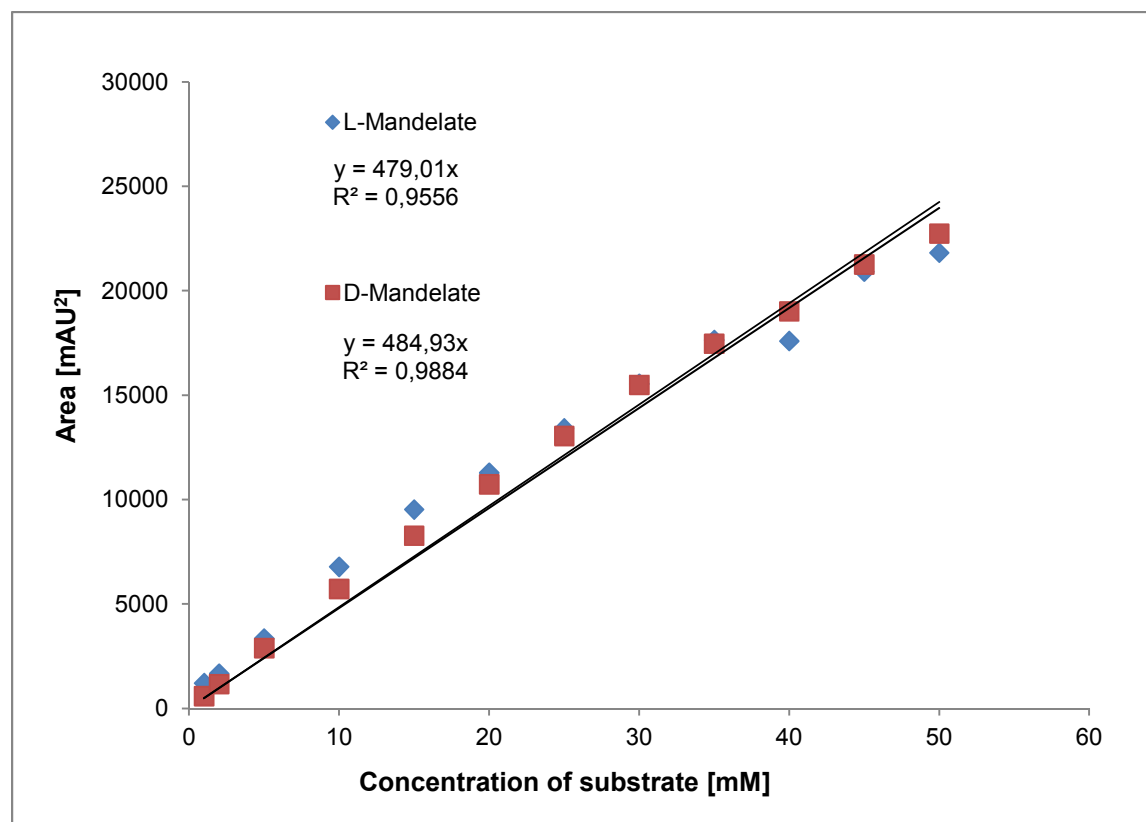
Figure 18: Calibration curve for D- and L mandelic acid quantification. Peak areas were linearly dependent on substrate concentration. Slopes were used for the calculation of analyte concentrations.

The reaction was optimized with regard to the LOX A95G concentration and the reaction time. Different enzyme concentrations and incubation times were used in reactions analyzed in figure 20 A. Hardly any conversion of DL-mandelic acid was detected with a catalyst loading of 0.05 or 0.1 µmol/min/mL and reaction times of 15 and 30 minutes. Similar results were obtained using 1 or 7.5 µmol/min/mL (U/mL) LOX A95G for reaction times of 15 or 30 minutes, respectively. Higher conversions were obtained with prolonged reaction times of 90 min for 1µmol/min/mL enzyme and 60 min for 7.5 µmol/min/mL enzyme. Interestingly, the lower catalyst loading led to higher conversions. Therefore, all following experiments were done with an enzyme concentration of 1 µmol/min/mL.
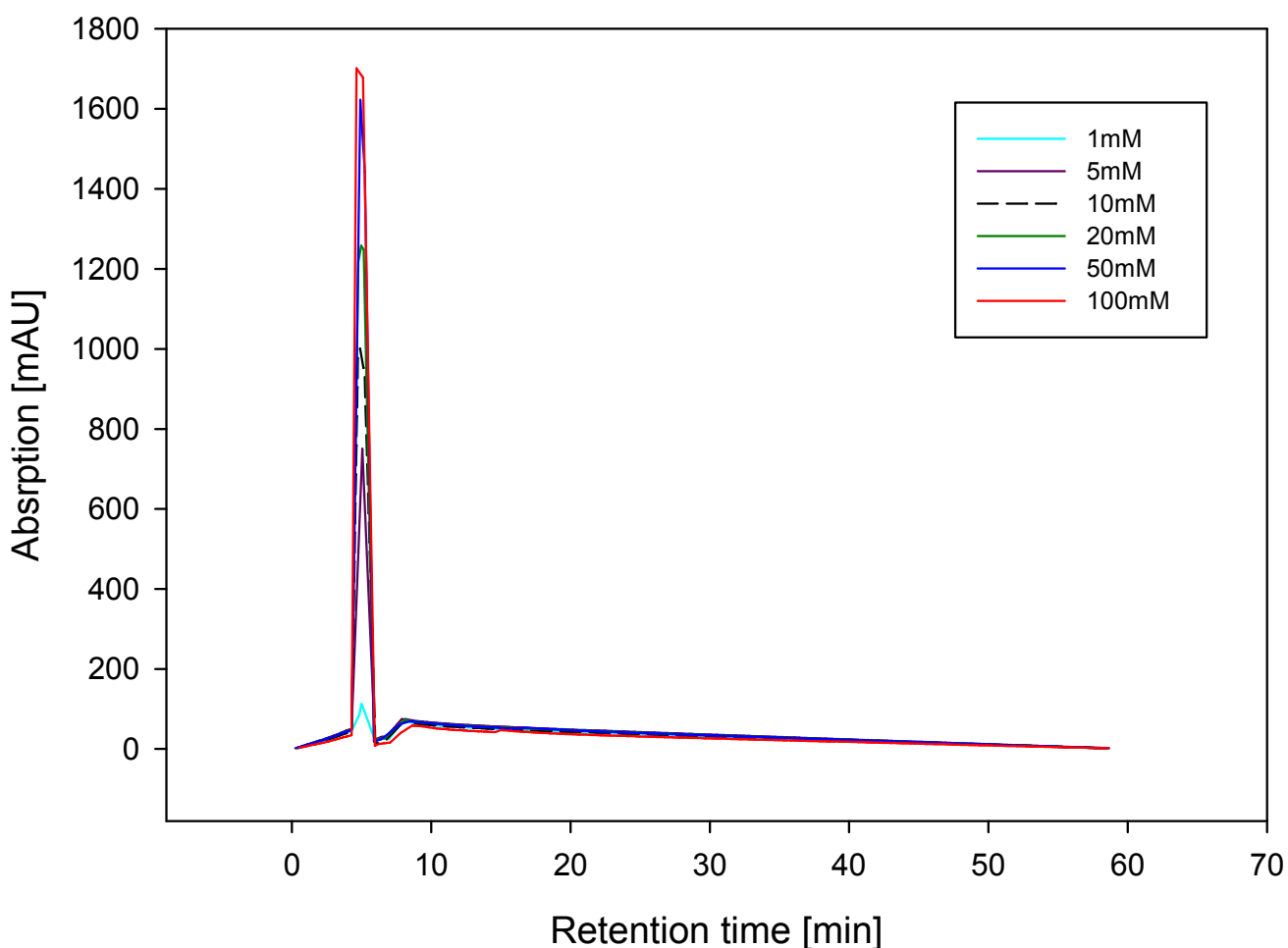
Figure 19: Standards of phenylglyoxylic acid in concentrations between 1 and 100 mM.
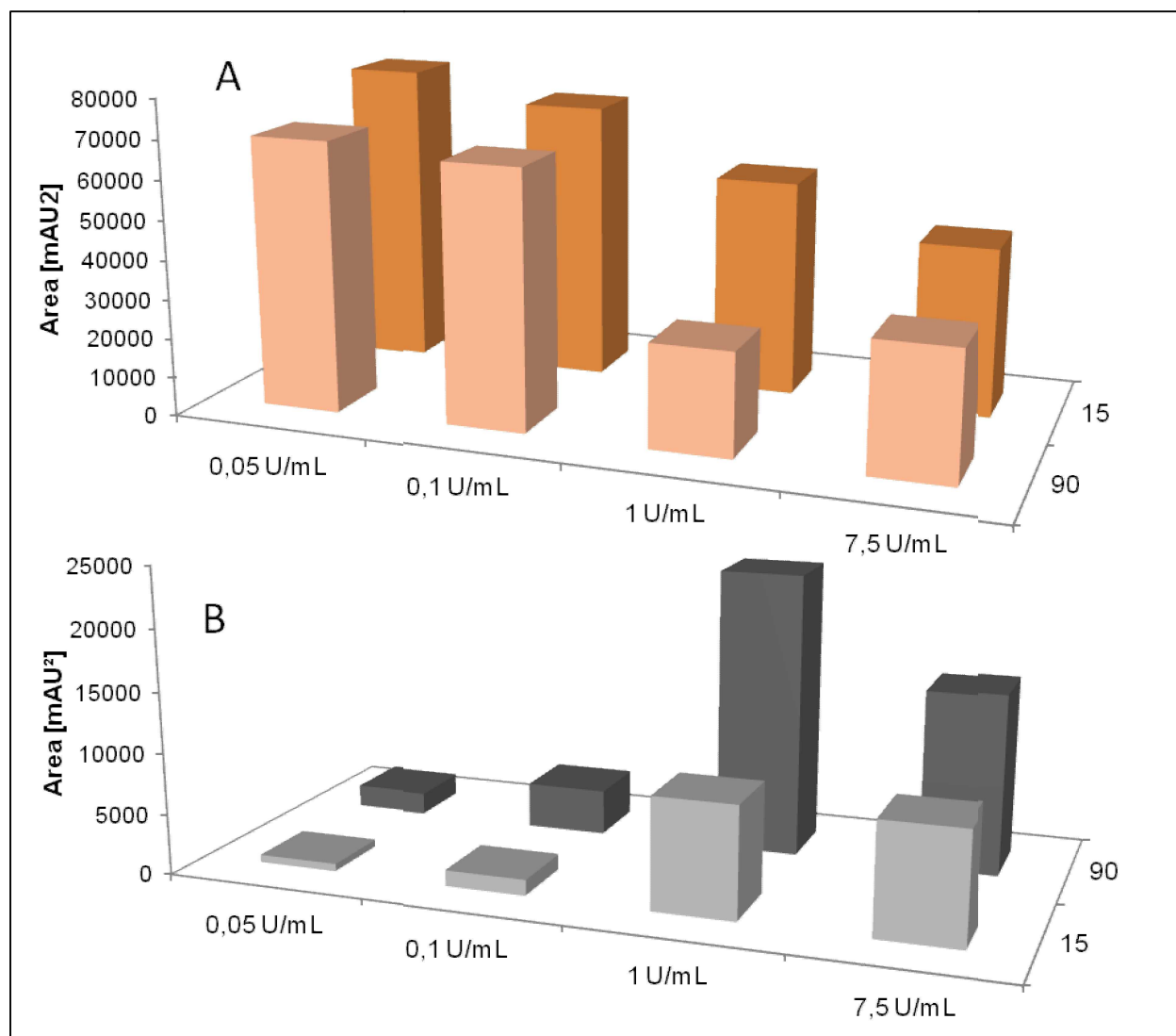
Figure 20: Optimization of DL-mandelic acid de-racemisation with regard to LOX A95G concentration and reaction time. X-axis represent the concentration of enzyme in µmol/min/mL (U/mL).The left y-axis shows the area in mAU² and the right y- axis shows the reaction time in minutes.

During the first analysis of the kinetic resolution of DL-mandelic acid, we also found out that benzoic acid is produced as a byproduct of PGA. The amount of production is dependent of the amount of enzyme used during the reaction. In figure 20 the relation of used enzyme (20 A) in comparison to the produced benzoic acid (20 B) is illustrated. The benzoic acid was not back-converted to D- or L-mandelic acid with addition of

NaBH4, and was therefore a stable substrate in the reaction. To avoid the production and guarantee a complete conversion of mandelic acid to the intermediate, catalase was added. Catalase blocks the reaction of benzoic acid production and therefore avoids a loss of substrate and final D-mandelic acid. The reaction mechanism of kinetic resolution therefore changed from the original from Oikawa et al. [Oikawa et al., 2001] and led to the new one depicted in figure 21.
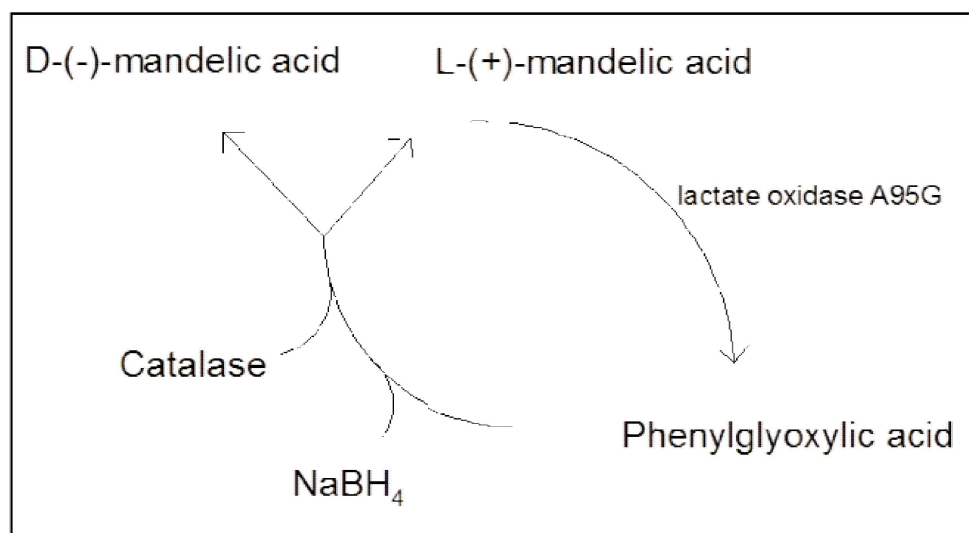
Figure 21: Reaction mechanism of DL-mandelic acid with the catalse enzyme added to avoid production of the by-product benzoic acid.

During the change of the HPLC column, pH 7.5 turned out as the optimal operational pH for HPLC analyses. The recommended pH for de-racemization is pH 8.0 [Oikawa et al., 2001]. A pH shift of the reaction mixture from 8.0 to 7.5 did not influence the productivity.

In table 7 a typical reaction course is shown. Because the intermediate PGA and L-mandelic acid were not baseline separated, the calculated values, area, concentration and percentage are based on D-mandelic acid.

Table 7: Values of measured samples of the de-racemization at pH 7.5. The concentration in the second row gives the amount of D-mandelic acid and the third row the same value in percentage.

Time [h:min]	Area	Conc. [mM]	%	
1	8412,3	17,35	43,37	Sample before adding NaBH4
01:17	9436,6	19,46	48,65	after addition of NaBH4
2	9052,5	18,67	46,67	before adding NaBH4
3	9230,8	19,04	47,59	before adding NaBH4
03:14	10325,9	21,29	53,23	after addition of NaBH4
4	10536,7	21,73	54,32	before adding NaBH4
04:10	10852,1	22,38	55,95	after addition of NaBH4
5	11203,8	23,10	57,76	before adding NaBH4
05:05	11785,2	24,30	60,76	after addition of NaBH4
05:15	12401	25,57	63,93	End of reaction

A closer look on table 7, especially on the row with the percentage, shows that there is no absolute conversion of L-mandelic acid to D-mandelic acid. Based on the assumption that we have a complete conversion of racemix mixture to the enantiomerically pure form, we calculated to need four cycles of addition of $NaBH_4$. However, after 5 cylces and addition of fresh enzyme after addition of $NaBH_4$ there is a total of 63.93% of D-mandelic acid.

3.5.   Crystallization & Structure

The harvested crystals were measured at the Stanford Synchrotron Radiation Lab with a Beamline 7-1 on 29 June 2011. Data were reduced using the HKL2000 program suite. Below the data collection can be observed with all relevant data about the crystal.

Data collection	
Unit cell dimensions	
a, b, c (Å)	122.59 124.36 106.89
α, β, γ (°)	90.00 124.29 90.00
Resolution range [Å]	50,00 – 1,65
No. of unique reflections	147349
Rmsd	0,764
Completeness [%]	98,2 (95.1%)
Rmerge	5.9% (37.1%)
Observations/unique reflections	581586/155981
I/sigma(I)	26.4 (4.1)
Refinement statistic	
R value [%]	17,6
Free R value	21,2
Deviations from ideal geometry	
Bond lengths [Å]	0,025
Bond angles [°]	2,200
ESU based on max. likelihood [Å]	0,062
Average B values [Å^2]	
Main-chain atoms	12.136

Side-chain atoms	14.986
FMN	10.312
Water molecules (705)	17.757
All atoms	13.730
Ramachandran Plot [%]	
Most favoured	96.6
Additionally allowed	3,0
Outliers	0,4

The structure of the mutant variant of LOX A95G is essentially identical in comparison with the structure of LOX WT (PDB entry: 2DU2). The structure has an average root-mean-square deviation (rmsd) for Cα backbone atoms of subunits, A, B, C, D, being 0.250, 0.174, 0.174, and 0.166 Å, respectively. These values indicate that there is no significant structural change as a result of the point mutation.

The model consists of four monomers, A, B, C, and D, in the asymmetric unit which gives the biological active unit. The residues 1-5 and 200 – 213 in subunit A; 1 – 5 and 202-215 in subunit B; 1-7 and 202-215 in subunit C and 1-7 and 202-205 in subunit D are not visible in the structure because of only partial electron density (Figure 22 A/B).

It belongs to the space group C1 2 1 at a resolution of 1,6Å. The overall fold of the enzyme forms a $(\beta/\alpha)_8$ barrel with the C-termini of each monomer located in the center of the tetramer.
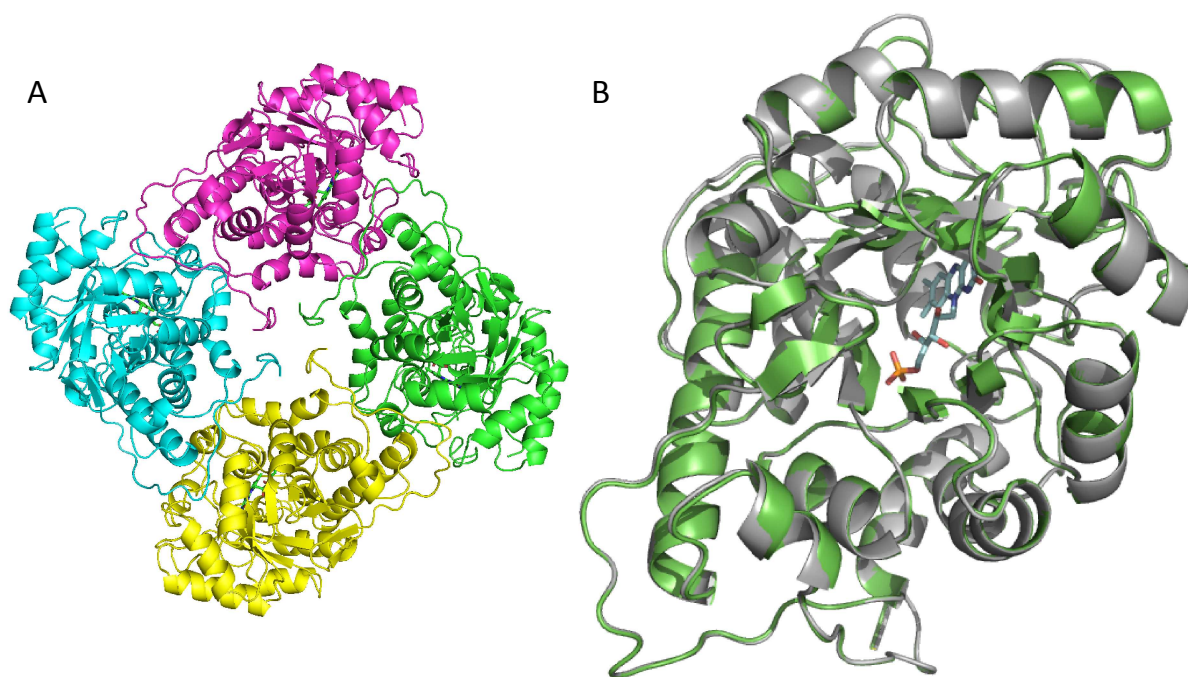
Figure 22: Crystal structure of the mutated variant of LOX A95G from *Aerococcus viridans* at 1.6Å resolution. (A) Tetramer form of the LOX A95G. (B) One subunit of the tetramer (green) in comparison to the wild type structure (grey). The FMN is located in the middle of the monomer colored in light blue.
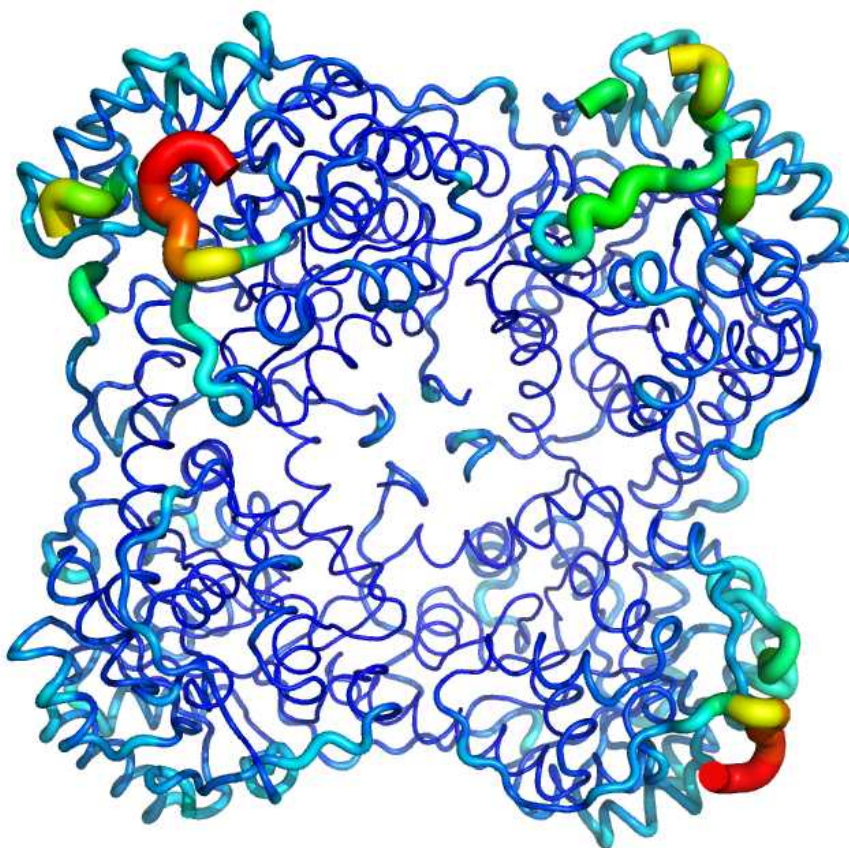
Figure 23: B-factor calculation for the tetramer structure of LOX A95G. The red regions show the lowest electron density regions.

Based on the B-factor calculation for the structure the regions with the highest B-factors are also these regions with the lowest electron densities which are not visible in structure further on (Figure 23 and 24).
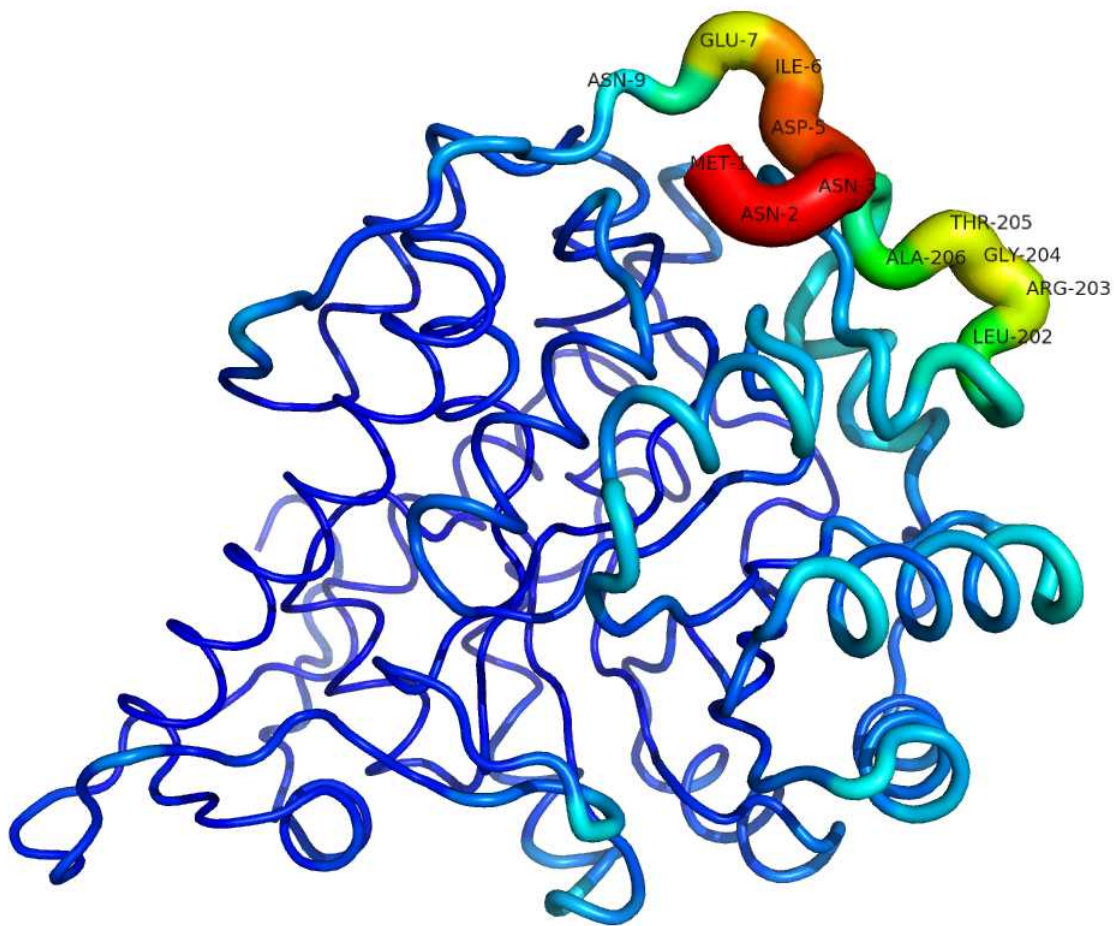
Figure 24: **B-factor calculation of the monomer in detail. Red to blue colors indicate B-values of high to low.**

With a closer look onto the mutated position of LOX (Figure 25) the neighboring Ala96 residue shows a conformational change. This change can be observed in every monomer of the mutant. However, this change was also found in one of the four monomers of WT LOX (PDB: 2DU2) but this is not the case in the wild type structure when pyruvate is present.
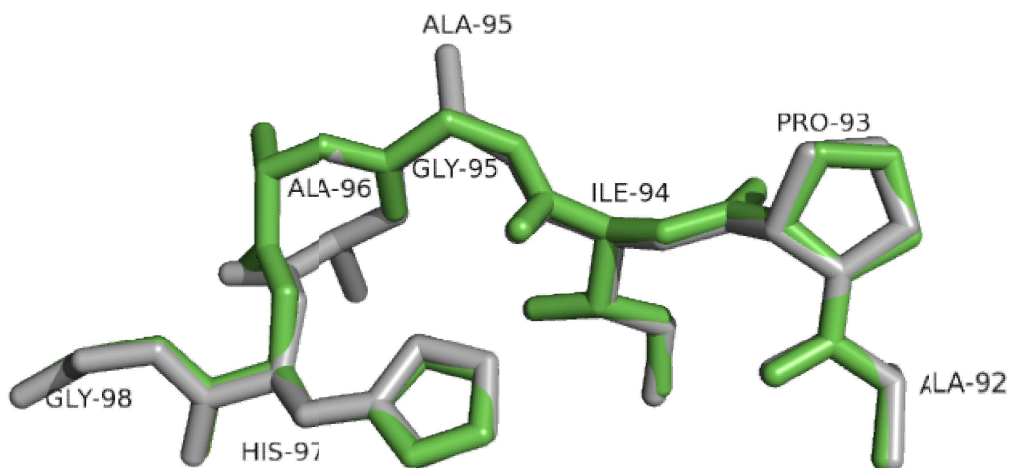
Figure 25: Comparison of the LOX WT (grey) and LOX A95G (green) mutant around position 95. The neighbouring amino acid at position 96 shows a conformational change in all four monomers of the mutated structure.

It seems that the change in conformation of position 96 also leads to a flip of the Tyr191 ring (Figure 26). Due to this flip all connections of Tyr191 to the surrounding Ala96 in the LOX WT are disappear (Figure 28) and new connections within the mutant variant are formed (Figure 27). Instead of residue Ala96 two other residues, namely Tyr40 and Leu211, are now in close vicinity of Tyr191 with 2.6 Å and 3.4 Å, respectively (caused by the conformational change).
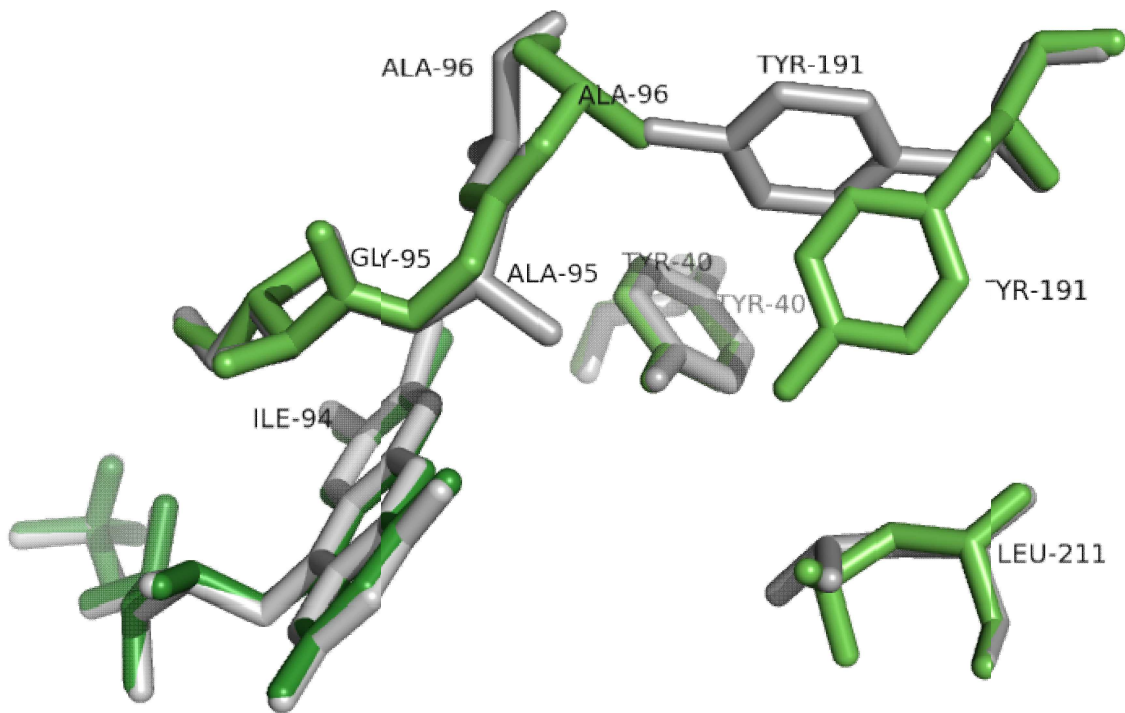
Figure 26: Comparison of active side residues of LOX WT and LOX A95G with the conformational change of the residue Tyr 191.
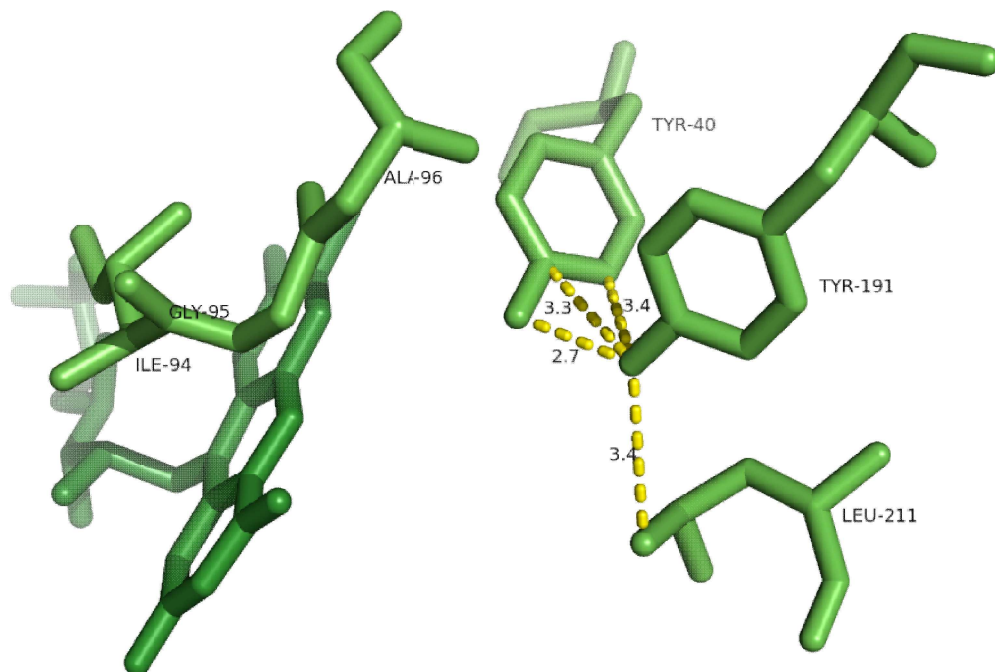
Figure 27: Calculated distances of the residue Tyr 191 in the active side of the LOX A95G.
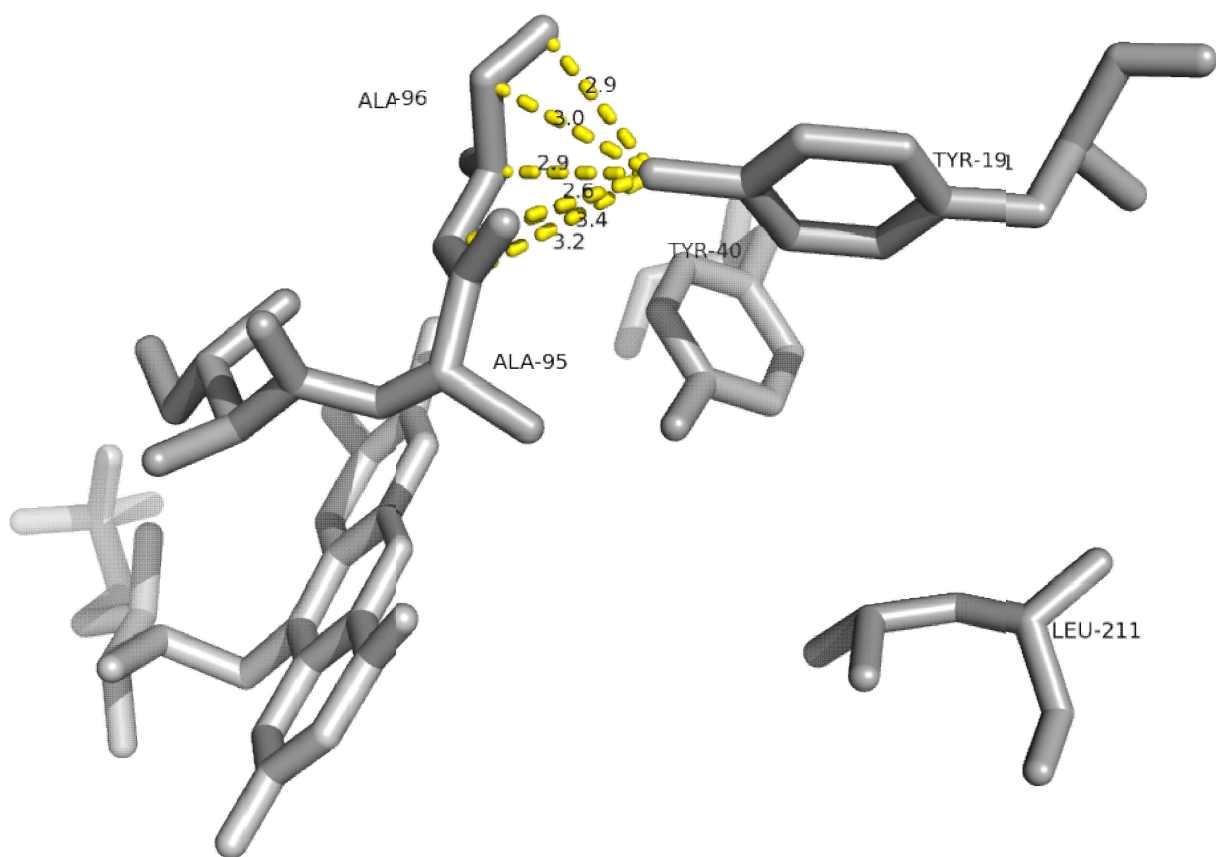
Figure 28: Active side residues of LOX WT with the distances of Tyr 191 to Ala 96.

Comparing LOX WT structure where pyruvate is missing with the structure where pyruvate is present (PDB code: 2E77) only a conformational change of residue Tyr191 can be found if pyruvate is part of the structure (Figure 29). Having a closer look into the structure of the wild type enzyme with bound pyruvate it could be observed that in monomer C no pyruvate is soaked and residue Tyr191 indicates the same conformation as the wild type from 2DU2 (picture not shown). These findings led us to the assumption that a conformational change of residue Tyr191 mainly occurs in the wild type after the substrate is bound to the active side.
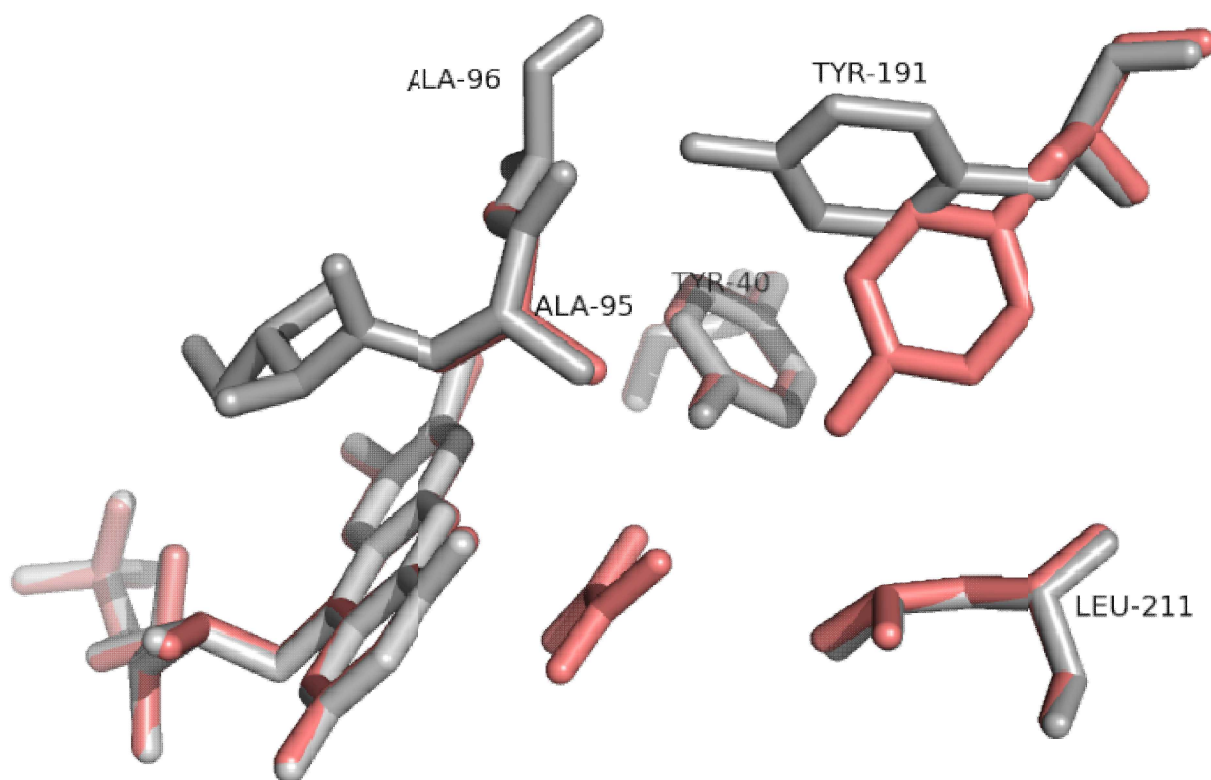
Figure 29: Comparison of two wild type structures. Grey residues show LOX WT from 2DU2 without any substrate bound. Red ones are from structure of 2E77 where pyruvate is soaked.

According to these observations we can also assume that the mutation of Ala95 leads to a permanent conformational change of residue Tyr191 and is therefore independent of substrate binding. The stabilization of residues Leu211 and Tyr40 residues are caused by the flip of Tyr191 which can lead to a more rigid structure concerning the transfer of substrates into the active site. Furthermore the lost connection to residue Ala96 widens the channel and facilitates the entrance for the substrates, which might be the reason why the LOX mutant reveals an increased substrate specificity concerning long chain α-hydroxy acids.

4. Conclusion

The purification of the LOX mutant A95G from *Aerococcus viridans* by using a three step process with ammonium sulfate precipitation, hydrophobic interaction and a strong ion exchange chromatography results in highly pure enzyme.

Kinetic studies prove that the mutant is not affected by L-mandelic acid whereas the wild type LOX is inhibited with a K_i of 0.30mM [Streitenberger et al., 2001].

Further characterizations show that the A95G mutant is highly stereospecific for L-mandelic acid, whereas D-mandelic acid neither acts an inhibitor nor is converted to the intermediate phenylglyoxylic acid.

Following the one-pot chemo-enzymatic de-racemization using the wild type LOX and the substrate DL-lactate [Oikawa et al., 2001] which gave a yield of 99% enantiomeric excess (ee), the method was applied to the A95G LOX and the substrate DL-mandelic acid. Here, the dynamic kinetic resolution of DL-mandelic acid to D-mandelic acid via PGA worked, in principal. However, no full conversion to D-mandelic acid was observed. After 5 cycles an ee of about 64% for D- mandelic acid was obtained in the reaction mixture.

Investigations on the structure of the mutated variant showed, that the change of the amino acid at position 95 had a severe change of substrate specificity, which can be explained by the more open channel around the active site.

The broader substrate specificity and x-fold increase of efficiency for several substrates renders A95G LOX interesting for several other applications.

5. References

Collaborative Computational Project 4, Acta Crystallogr. D50 (1994) 760-763

Cornforth J.W. (1959). Fatty Acids and Cholesterol considered as Chemical Processes. *Journal of Lipid Research*, *1*(1), 3-28.

Cunane, L. M., Barton, J. D., Chen, Z.-wei, Lê, K. H. D., Amar, D., Lederer, F., & Mathews, F. S. (2005). Crystal structure analysis of recombinant rat kidney long chain hydroxy acid oxidase. Biochemistry, 44(5), 1521-1531.

Dewanti, A. R., & Mitra, B. (2003). A transient intermediate in the reaction catalyzed by (S)-mandelate dehydrogenase from Pseudomonas putida. Biochemistry, 42(44), 12893-12901. Retrieved from http://www.ncbi.nlm.nih.gov/pubmed/14596603

Emsley P., Lohkamp B., Scott W., Cowtan K. (2010) Features and Development of Coot: ACTA CRYSTALLOGRAPHICA SECTION D-BIOLOGICAL CRYSTALLOGRAPHY 66, 486-501.

Ghisla, S., Ogata, H., Massey, V., Schonbrunn, A., Abeles, R. H., & Walsh, C. T. (1976). Kinetic studies on the inactivation of L-lactate oxidase by the acetylenic suicide substrate] 2-hydroxy-3-butynoate. Biochemistry, 15(9), 1791-1797

Ghisla, S., Universittit, D., Konstanz, D., & Germany, W. (1977). Studies on the Mechanism Lactate Oxidase of Action of the Flavoenzyme. Biochemistry, 252(19), 1798-1807.

Huang, J., Li, J., Yang, Y., Wang, X., Wu, B., Anzai, J.-ichi, Osa, T., et al. (2008). Development of an amperometric l-lactate biosensor based on l-lactate oxidase immobilized through silica sol–gel film on multi-walled carbon nanotubes/platinum

nanoparticle modified glassy carbon electrode. Materials Science and Engineering: C, 28(7), 1070-1075.

Kim, M.-J., Chung, Y. I., Choi, Y. K., Lee, H. K., Kim, D., & Park, J. (2003). (S)-selective dynamic kinetic resolution of secondary alcohols by the combination of subtilisin and an aminocyclopentadienylruthenium complex as the catalysts. Journal of the American Chemical Society, 125(38), 11494-11495.

Leiros, I., Wang, E., Rasmussen, T., Oksanen, E., Repo, H., Petersen, S. B., Heikinheimo, P., et al. (2006). The 2.1 A structure of Aerococcus viridans L-lactate oxidase (LOX). Acta crystallographica. Section F, Structural biology and crystallization communications, 62(Pt 12), 1185-90.

Massey, V., Ghisla, S., & Kieschkeg, K. (1980). Studies on the Reaction Mechanism of Lactate Oxidase. Biological Chemistry, 255(7), 2796-2806.

Mattevi, A., Vanoni, M. A., Todone, F., Rizzi, M., Teplyakov, A., Coda, A., Bolognesi, M., et al. (1996). Crystal structure of D-amino acid oxidase: a case of active site mirror-image convergent evolution with flavocytochrome b2. Proceedings of the National Academy of Sciences of the United States of America, 93(15), 7496-7501.

Murshoduv G.N., Vagin A.A., Dodson E.J. (1997) Refinement of macromolecular structures by the maximum-likelihood method, Acta Crystallogr. D53, 240-255

Oikawa, T., Mukoyama, S., & Soda, K. (2001). Chemo-enzymatic D-enantiomerization of DL-lactate. Biotechnology and bioengineering, 73(1), 80-2.

Pàmies, O., & Bäckvall, J.-E. (2003). An efficient route to chiral alpha- and beta-hydroxyalkanephosphonates. The Journal of Organic Chemistry, 68(12), 4815-4818.

Rao, K. S., & Lederer, F. (1998). About the pKa of the active-site histidine in flavocytochrome b2 (yeast L-lactate dehydrogenase). Protein Science, 7(7), 1531-1537. Cold Spring Harbor Laboratory Press.

Schnell, B., Faber, K., & Kroutil, W. (2003). Enzymatic Racemisation and its Application to Synthetic Biotransformations. Advanced Synthesis Catalysis, 345(67), 653-666.

Schonbrunn, A., Abeles, R. H., Walsh, C. T., Ghisla, S., Ogata, H., & Massey, V. (1976). The structure of the covalent flavin adduct formed between lactate oxidase and the suicide substrate 2-hydroxy-3-butynoate. Biochemistry, 15(9), 1798-1807.

Sobrado, P., & Fitzpatrick, P. F. (2003). Solvent and primary deuterium isotope effects show that lactate CH and OH bond cleavages are concerted in Y254F flavocytochrome b2, consistent with a hydride transfer mechanism. Biochemistry, 42(51), 15208-15214.

Soda, K., Oikawa, T., & Yokoigawa, K. (2001). One-pot chemo-enzymatic enantiomerization of racemates. Journal of Molecular Catalysis B: Enzymatic, 11(4-6), 149-153.

Streitenberger, S. A., López-Mas, J. A., Sánchez-Ferrer, A., & García-Carmona, F. (2001). Non-linear slow-binding inhibition of Aerococcus viridans lactate oxidase by Cibacron Blue 3GA. Journal of Enzyme Inhibition, 16(4), 301-312.

Sun, W., Williams, C. H., Jr., and Massey, V. (1996). Site-directed Mutagenesis of Glycine 99to Alanine in L-Lactate Monooxygenase from Mycobacterium smegmatis. Journal of Biological Chemistry, 271(29), 17226-17233.

Turner, N. J. (2004). Enzyme catalysed deracemisation and dynamic kinetic resolution reactions. Current Opinion in Chemical Biology, 8(2), 114-119.

Umena, Y., Yorita, K., Matsuoka, T., & Kita, A. (2006). The crystal structure of L-Lactate oxidase from Aerococcus viridans at 2.1 resolution reveals the mechanism of strict substrate recognition. Biochemical and, 350, 249-256.

Vagin A.A., Steiner R.A., Lebedev A.A., Potterton L., McNicholas S., Long F., Murshudov G.N. (2004) REFMAC5 dictionary: organization of prior chemical knowledge and guidelines for its use: ACTA CRYSTALLOGRAPHICA SECTION D-BIOLOGICAL CRYSTALLOGRAPHY 60, 2184-2195.

Walsh, C. (1973). Studies on the Mechanism Lactate of Action of the Flavoenzyme. Journal of Biological Chemistry, 248(20), 7049-7054.

Walsh, Christopher T., Schonbrunn, A., Abeles, R. H. (1971). Studies on the Mechanism of Action of D-Amino Acid Oxidase. *Journal of Biological Chemistry*, *246*(22), 6855-6866.

Wuyts, S., De Temmerman, K., De Vos, D., & Jacobs, P. (2003). A zeolite-enzyme combination for biphasic dynamic kinetic resolution of benzylic alcohols. Chemical Communications, (15), 1928-1929.

Yorita, K., Aki, K., Ohkuma-Soyejima, T., Kokubo, T., Misaki, H., & Massey, V. (1996). Conversion of L-lactate oxidase to a long chain alpha-hydroxyacid oxidase by site-directed mutagenesis of alanine 95 to glycine. The Journal of biological chemistry, 271(45), 28300-5.

Yorita, K., Janko, K., Aki, K., Ghisla, S., Palfey, B. a, & Massey, V. (1997). On the reaction mechanism of L-lactate oxidase: quantitative structure-activity analysis of the reaction with para-substituted L-mandelates. *Proceedings of the National Academy of Sciences of the United States of America*, *94*(18), 9590-5.

6. List of Abbreviations and Symbols

$(NH_4)_2SO_2$	Ammoniumsulfate
A,Ala	Alanine
A96G	Mutant variant of LOX
AAP	4-aminoantipyrine
Amp	Ampicillin
Av	*Aerococcus viridans*
BSA	Bovine serum albumin
CIP	Cleaning in Place
CV	Column volume
DAO	D-amino acid oxidase
DBS	Dodecylbenzensulfonic acid
DKR	Dynamic kinetic resolution
DMA	N,N- Dimethylaniline
E.Coli	*Escherichia Coli*
FMN	Flavin mononucleotide
G, Gly	Glycine
GLO	Glycolate oxidase
H_2O	water
H_2O_2	Hydrogen peroxide
HIC	hydrophobic interaction chromatography
HPLC	High pressure liquid chromatograohy
IPTG	Isopropyl- -D-1-thiogalactopyranoside
K_2PO_4	Potassium-hydrogen-phosphate
k_{cat}	Turnover number
KCl	Sodiumchloride
KH_2PO_4	sodium *di*-hydrogen phosphate
K_M	Michaelis-Menten constant
LMO	Lactate monooxigenase
LOX	L-lactate oxidase

MgSO$_4$	Magnesiumsulfate
min	minutes
NaBH$_4$	Sodium borohydrid
NaOH	Sodium hydroxide
OD$_{600}$	Optical density at 600 nm
PGA	Phenylglyoxylic acid
PO$_4$ buffer	Phosphate buffer
POD	Horseradisch peroxidase
rpm	Rounds per minute
RT	Room temperature
TFA	trifluoroacetate
Tris	2-amino-2-hydroxymethyl-propane-1,3-diol
WT	Wild type LOX

Appendix

Comprehensively explicated and additionally used Methods and Materials

DEAE Cellulose chromatography

Purification with DEAE was not satisfactory as can be seen in the figure below (Figure 30). The SDS PAGE gel shows the protein after the different steps of purification and the crude extract after French press. The last two lanes show the protein purified with DEAE. There are plenty of other proteins in the fractions.
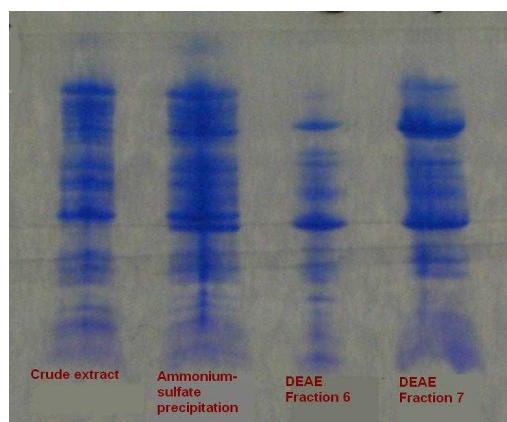
Figure 30: SDS PAGE of the different steps of purification with DEAE column (last two lanes).

In fraction 6 of the DEAE purification (Figure 31), the purity of the protein is higher than in fraction 7. Nevertheless, both fractions had to be pooled to guarantee the highest yield of useful protein. So it can be assumed that the purification with DEAE shows not enough purity of the protein which leads to a change of method for purification.
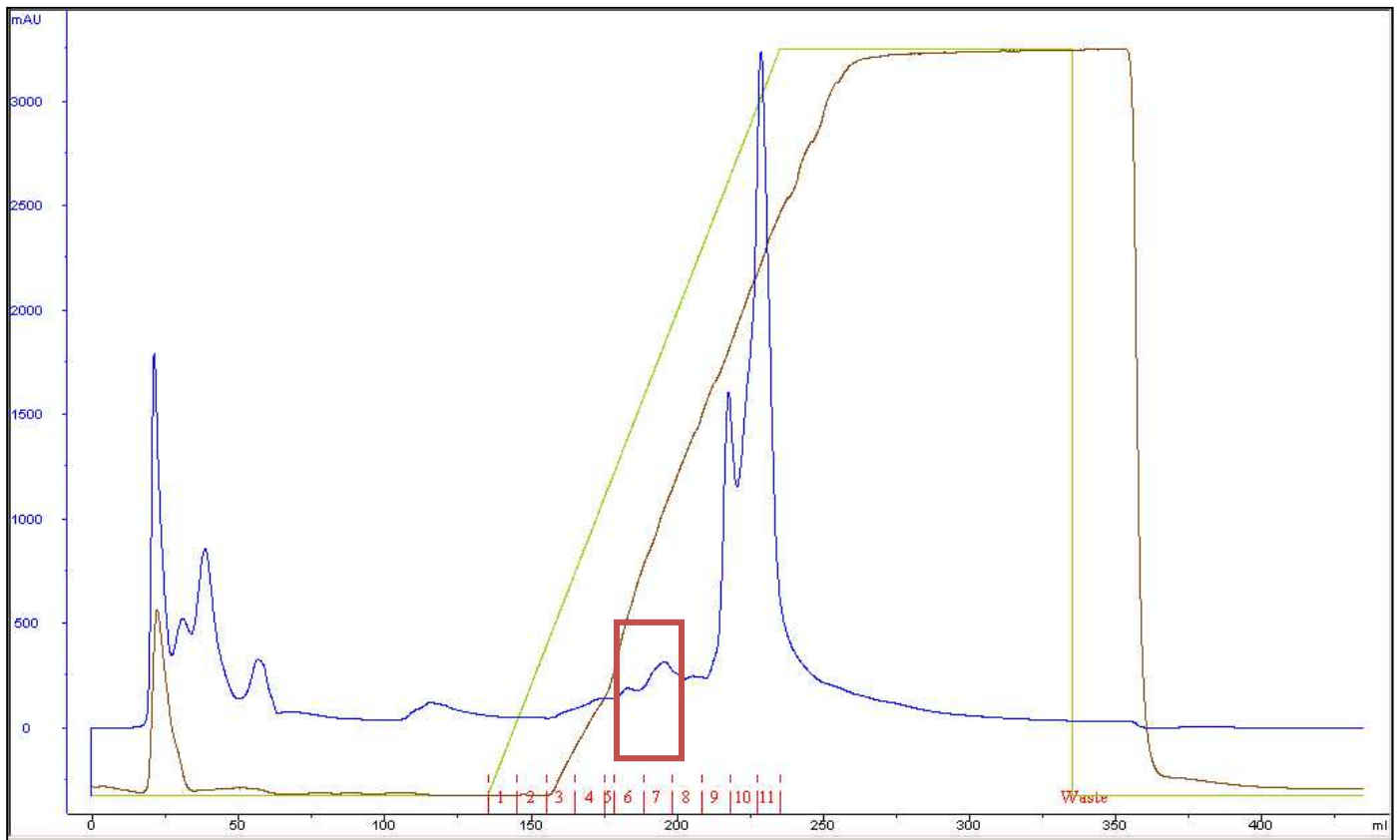
Figure 31: Chromatogram of DEAE purification of A95G LOX. The red box show the fraction in which activity was measured and also these fractions were pooled. The x-axis gives volume used for the purification, y-axis gives UV-signal (mAU). Blue line: UV-signal; green line: concentration of elution buffer (50mM KH$_2$PO$_4$ + 1M KCl); brown line: conductivity (mS/cm)

Ammonium sulfate precipitation

- Precipitation of Protein occurs on ice with careful stirring. The Ammonium sulphate solution is added drop wise to the protein.
- Carful stirring half an hour on ice.
- Centrifugation at 4°C for 1 hour.
- Supernatant is collected and pellet is thrown away.
- Ready to use for HIC

Hydrophobic Interaction Chromatography (HIC)

Cleaning in Place

1. 1 CV H_2O
2. 1 CV 0.5M NaOH
3. 2 CV H_2O

Purification

1. Equilibration: 1CV with washing buffer
2. Loading sample: the smaller the volume the better it is
3. Washing: 2-3 CV with washing buffer (A)
4. Elution: Gradient with buffer B
   - 0 – 50% B 128mL (2CV)
   - 50- 80% B 128mL (2CV)
   - 80- 100% B 128mL (2CV)
5. Washing: 2-3 CV with 100%B
6. Re-equilibration: washing buffer (A) until UV and conductivity are flat lined

The protein from the purification with HIC has to be desalted from $(NH_4)_2SO_4$ to guarantee the binding of the protein onto the Mono Q column. Otherwise it will not bind and be washed out with the first CV.

Ion exchange chromatography Mono Q

Purification

1. Equilibration: 5-10 CV with washing buffer or until UV signal and conductivity give a constant flat line (~ 0)
2. Loading sample: the smaller the volume of loading the better it is
3. Washing: 5-10CV with washing buffer (A) (UV signal and conductivity = flat lined)
4. Elution: Gradient to 1000% B (stepwise)
5. Washing: 2-5 CV with 100% B
6. Re-equilibration: 5-10 CV (UV signal and conductivity = flat lined)

Cleaning in Place (CIP)

1. 2CV 2M KCl
2. 4CV 1M NaOH
3. Dest. Water until Conductivity is flat lined
4. 2CV 2M KCl
5. 2CV H2O
6. 4CV washing buffer (start buffer; A)
   2 CVs H_2O

   2-5 CVs 20% Ethanol (storing buffer)

A comprehensive list of used instruments and devices is shown in table 8.

Table 8: Instruments and devices

AEC column	MonoQ, GE Healthcare Life Sciences
Agarose gel accessories	Chamber Mini-Sub Cell (BIORAD); Model 200/2.0 Power Supply (BIORAD)
Autoclaves	Varioklav; Fedegari; Systec; Certoclav
Beakers	Schott Duran®, Germany
Cold storage room	Lassacher Großkücken, 4°C
Cuvettes	Plastic: Sarstedth AG & Co., Germany; Quarz: Hellma® GmbH & Co. KG
Fermenter ans accessories	B.Braun Biotech International Biostat®C, Type CT5-2 Biostat®CT, Innova Air Tech Instruments 1313 Fermentation Monitor
Flasks	Schott Duran® , Germany
FPLC System	ÄKTA, Amersham Bioscience UPC- 900 P-920
Freezer	Elin & Liebherr (-25°C); Thermo Scientific Revco Legaci (-70°C)
Glass bottles	Schott Duran®, Germany

Glucose testing stripes	Diabur Test 5000, Roche Diagnostics
HIC column	Phenyl Sepharose TM , Fast Flow, GE Healthcare
Incubator 37°C	Heraeus® Instruments GmbH
Laminar flow	BIOAIR® Euroclean® Group, Aura 2000 M.A.C4, Italy
Magnetic stirrer	Heidolph MR 3001K; Heidolph MR3000D
pH-measurement	Biotrode electrode, Hamilton Bonaduz AG; Metrom 691 pH-meter, METROHM AG
Photometer	Varian Cary® 50 Bio UV-Visible Spectrophotometer
Pipette tips	Ultratip Greiner Bio-one 200µL/ 1000µL
Pipettes	Pipetman Gilson Inc., USA; P20N, P200N, P1000N
Reaction tubes 1.5 mL	Sarstedt AG & Co., Germany
Scales	Acculab vicon/ Analytic, Sartorius Stedim Biotech GmbH, Germany
SDS gels	SDS PhastGel TM Gradient 8-25, GE Healthcare Life Sciences; Pharmacia High Speed Electrophoresis System, Pharmacia Biotech
Thermomixer	Eppendorf compact, Germany; Eppendorf comfort, Germany
Vivaspin 500, 20	10kDa cutoff, Vivascience AG, Hannover, Germany
Water purification system	TKA Wasseraufbereitungssysteme GmbH, Germany

All used chemicals and suppliers are listed in table 9.

Table 9: Reagents, chemicals and suppliers

2-chloro mandelic acid	Sigma Aldrich Corp.
2-fluoro-mandelic acid	Sigma Aldrich Corp.
3,3- Dimethylglutaric acid	Sigma Alrich Corp.

4-fluoro-mandelic acid	Sigma Aldrich Corp.
Ammonium sulfate	Sigma Aldrich Corp.
di- Potassium hydrogen phosphate	Carl Roth GmbH + Co KG
Glucose * H2O	Carl Roth GmbH + Co KG
L-(+)-lactic acid	Sigma Aldrich Corp.
L-2-hydroxy-3-methylbutyric acid	Sigma Aldrich Corp.
L-2-hydroxybutyric acid	Sigma Aldrich Corp.
L-2-hydroxyisocaproic acid	Sigma Aldrich Corp.
L-glyceric acid	Sigma Aldrich Corp.
L-glycolic acid	Sigma Aldrich Corp.
L-mandelic acid	Sigma Aldrich Corp.
LMW Protein Standard	GE Healthcare Life Sciences
Loading dye	Germentas- Thermo Fisher Scientific Inc.
Magnesium sulfate * 7H2O	Carl Roth GmbH + Co KG
N,N- Dimethylaniline	Sigma Aldrich Corp.
para-hydroxy mandelic acid	Sigma Aldrich Corp.

para-methoxy-mandelic acid	Sigma Aldrich Corp.
Peptone	Carl Roth GmbH + Co KG
pH calibration solution pH 4.01	Hamilton Nr.1312829
pH calibration solution pH 7.00	Hamilton Nr.1314185
Poly(propylene glycol)	Carl Roth GmbH + Co KG
Potassium chloride	Carl Roth GmbH + Co KG
Potassium di-hydrogen phosphate	Carl Roth GmbH + Co KG
Potassium hydroxide	Merck GmbH
Roti®Quant Protein Quantitation	Carl Roth GmbH + Co KG
SDS	Carl Roth GmbH + Co KG
Sodium hydroxide	Carl Roth GmbH + Co KG
TRIS	Carl Roth GmbH + Co KG
Yeast Extract	Carl Roth GmbH + Co KG

Figures

Tables